Testing modes of exhumation in collisional orogens: Synconvergent channel flow in the southeastern Canadian Cordillera

Félix Gervais* and Richard L. Brown
DEPARTMENT OF EARTH SCIENCES, CARLETON UNIVERSITY, 2125 HERZBERG BUILDING, 1125 COLONEL BY DRIVE, OTTAWA, ONTARIO K1S 5B6, CANADA

ABSTRACT

This study investigates exhumation processes in collisional orogens. A critical test between three modes of exhumation is presented based on a review of quantitative numerical and analogue modeling studies. The test is applied to the large tract of migmatites surrounding the Monashee Complex in the southeastern Canadian Cordillera. It reveals that the extensive and multidisciplinary database of this region is entirely compatible with the synconvergent channel-flow mode but not with critical wedge and gravitational collapse modes. We propose that a partially molten channel decoupled from its lid and base and started to flow in the middle crust toward the foreland at 100–90 Ma. A steady-state channel-flow system was established for the following ~30 m.y., during which rocks at the front of the channel were exhumed to upper-crustal levels as they flowed above an underthrusting basement ramp. Flow was accommodated by oppositely verging shear zones bounding the channel, by internal ductile deformation, and by shortening in the foreland belt. The locus of flow migrated downward to exhume rocks of the Monashee Complex between 60 and 50 Ma by a similar process. The southeastern Canadian Cordillera thus constitutes an excellent natural analogue for the channel-flow model. In contrast to the commonly held view of large-magnitude extension and core complex formation, the role of extension was limited to the final ~10–15 km of exhumation after 50 Ma.

LITHOSPHERE; v. 3; no. 1; p. 55–75. doi: 10.1130/L98.1

INTRODUCTION

The mechanisms that lead to the exposure of large areas of high-grade rock in the hinterland of collisional orogens are long-standing tectonic issues (e.g., Ring et al., 1999). The uplift of rock relative to Earth's surface is referred to as "exhumation" (cf. England and Molnar, 1990). It can occur during convergence or during postcollisional extension. It commonly involves a complex interaction among erosion, normal faulting, and underplating (e.g., Ring et al., 1999), and may involve crustal decoupling and ductile flow (e.g., Beaumont et al., 2001). It is possible to group the various exhumation processes into three main modes: postconvergence gravitational collapse (cf. Rey et al., 2001), synconvergent orogenic wedges (e.g., Platt, 1986; Dahlen, 1990), and synconvergent channel flow and ductile extrusion (e.g., Beaumont et al., 2001).

The southeastern Canadian Cordillera (Fig. 1), with its easy access and excellent exposure, is one of the most studied collisional orogens exposing a large tract of midcrustal migmatites. Although it has been cited as a type example of postconvergent gravitational collapse resulting in extensional metamorphic core complexes (Coney and Harms, 1984; Parrish et al., 1988; Vanderhaeghe and Teyssier, 1997; Teyssier and Whitney, 2002; Teyssier et al., 2005; Rey et al., 2009), other workers have argued that a significant portion of the exhumation path occurred during convergence in an orogenic wedge (Brown and Journeay, 1987; Parrish, 1995; Brown, 2004), or by ductile extrusion and channel flow (Scammell, 1993; Johnston et al., 2000; Williams and Jiang, 2005; Brown and Gibson, 2006; Glombick et al., 2006a; Kuiper et al., 2006). It therefore provides an excellent natural laboratory in which to devise and apply diagnostic tests for the different processes that may contribute to exhumation processes in collisional orogens.

In this contribution, we first devise such a test by extracting a set of diagnostic criteria from relevant numerical and analogue modeling studies. It is then applied to rocks surrounding the Monashee Complex in the southeastern Canadian Cordillera. Only one model passes the critical test.

*Current address: Department of Earth & Planetary Sciences, McGill University, Montreal, Quebec H3A 2A7, Canada; felix.gervais@mcgill.ca.

DIAGNOSTIC CRITERIA OF EXHUMATION MODES

Our diagnostic criteria were derived from a compilation of the main characteristics of 14 models that provide predictions about the evolution of structural and metamorphic patterns (Table 1). We found that the shape of pressure-temperature (*P-T*) paths and absolute peak *P-T* conditions are not sufficiently diagnostic of the processes involved. For example, near-isothermal decompression paths can be produced in all three modes, depending on modeling parameters. In contrast, the spatial distribution of finite-strain patterns, cooling ages, and *P-T*-time (*t*) paths, as well as metamorphic field gradients and the timing of motion along reverse and normal shear zones, are diagnostic. Along with the set of criteria, Figure 2 presents the three models from each category that are most consistent with the overall geometry of the area surrounding the Monashee Complex in the southeastern Canadian Cordillera, which is illustrated on the cross section of Figure 3A.

From the subduction to the collision phase, convergent orogens have a wedge shape that is consistent with the critical-taper theory (e.g., Platt, 1986; Dahlen, 1990). In thermomechanical models of continental collision, in which the mantle lithosphere on the prowedge side detaches and subducts beneath a stationary retromantle (e.g., Willett et al., 1993), orogens develop a bivergent wedge geometry bounded by two oppositely verging shear zones. In the absence of erosion, exhumation is limited,

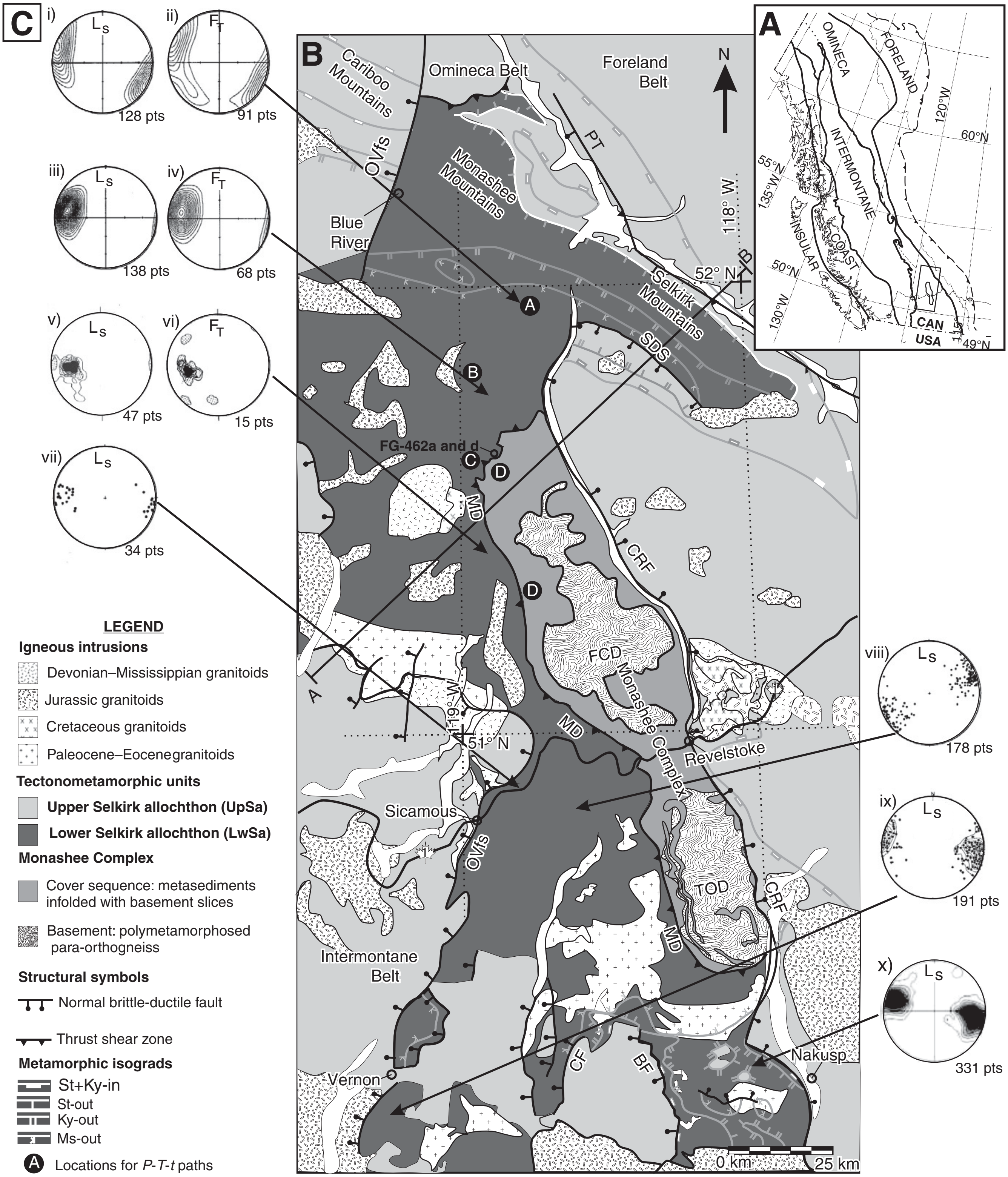

Figure 1. Tectonometamorphic map of the southeastern Canadian Cordillera surrounding the Monashee Complex. (A) The five morphogeological belts of the Canadian Cordillera (modified from Wheeler and McFeely, 1991) and the location of the study area. (B) Simplified geological map showing the three tectonometamorphic units, the main intrusive suites, and the traces of isograds. (C) Equal-area, lower-hemisphere projections for stretching lineations (L_s) and transposed folds (F_T). Structural data: (i–iv) from Scammell (1993); (v–vi) from Journeay (1986); (vii–viii) from Johnson (2006); (ix) from Glombick et al. (2006a); and (x) from Lemieux (2006). Circles with capital letters A–D are specific locations discussed in the text. Abbreviations: OVfs—Okanagan Valley fault system; PT—Purcell thrust; SDS—Selkirk detachment system; MD—Monashee décollement; CRF—Columbia River fault; FCD—Frenchman Cap dome; TOD—Thor-Odin dome; CF—Cherry fault; BF—Beaven fault.

TABLE 1. COMPILATION OF CHARACTERISTICS OF THE THREE MAIN EXHUMATION MODES IN COLLISIONAL OROGENS

Model	General characteristics	*P-T-t* path shape	Metamorphic field gradient	Absolute peak *P-T*	Spatial distribution finite strain patterns	Spatial distribution cooling ages	Spatial distribution *P-T-t* paths	Timing of shear zones, reverse vs. normal
Gravitational collapse								
Rey et al. (2009) Thermomechanical MCC Strain rate and presence of melt	Nearly symmetric HT dome cored by migmatites surrounded by suprastructure	IT-D to C-D	↑T+↑P → dome core sharp gradient with suprastructure	Variable	Outward-verging shearing at margins. Horizontal flattening in dome core	Younger → dome core	↓T, ↓P throughout	Reverse > normal
Tirel et al. (2006) Thermomechanical MCC Conditions for development	Asymmetric HT dome surrounded by suprastructure. Vergence of normal detachment varies	n.a.	↑T+↑P → dome core sharp gradient with suprastructure	n.a.	Outward-verging shearing at margins. Horizontal flattening in dome core	Younger → dome core	↓T, ↓P throughout	Reverse > normal to reverse = normal if channel flow
Tirel et al. (2009) Thermomechanical Sequential MCC Figure 5	Early dome asymmetric and flattened; overlies late symmetric dome	n.a.	↑T+↑P → in first dome sharp gradient with suprastructure	n.a.	Coeval reverse-normal shear zones bounding flattened first dome. Outward verging shearing at margins of second dome. Horizontal flattening dominates	Younger in second dome	↓T, ↓P throughout	Reverse = normal in first dome Reverse > normal in second dome
Brun et al. (1994) Analogue MCC	Migmatite dome bounded by outward-verging shear zones. Suprastructure dissected by normal faults	IT-D	↑T+↑P → dome core sharp gradient with suprastructure	n.a.	Outward-verging shearing at margins. Horizontal flattening in dome core	Younger → detachment	↓T, ↓P throughout	Reverse > normal
Jamieson et al. (2002) Stopped convergence LHO-77 45–90 m.y.	Antiform in HW of retro-shear zone	IT-D to C-D	Early exhumed HT rocks in HW of retro-shear zone of the wedge and late exhumed MT rocks on the prowedge side	400–700 °C 500–1200 MPa	Significant horizontal flattening throughout hinterland Reverse and normal shear zones bounding the base and roof of a midcrustal channel flowing toward the prowedge side	Older → HW retro-shear zone Younger → late exhumed area	↓T, ↓P throughout	Reverse > normal Except at the roof of the midcrustal channel
Jamieson et al. (2010) Stopped convergence Lower-crustal heterogeneous viscosities GO-ST87	Foreland fold-and-thrust belt to detached lower-crustal hot fold nappes to channel made of heterogeneous assemblage of mid- to lower-crustal rocks. Not exhumed after 25 m.y. of extension	IB-C to C-D	Large tract of migmatites with different *P-T-t* histories	660–730 °C 700–1000 MPa	MCC with outward-verging shearing at margins Normal shear zone between molten midcrust and strong lower crust Significant horizontal flattening throughout hinterland	n.a.	↓T, ↓P throughout	Reverse > normal but lower-crustal normal shearing coeval with thrusting in the foreland
Orogenic wedges								
Batt and Braun (1999) Thermomechanical	Exhumed HT retro-shear zone	IT-B, IT-D	Sharp in the FW of the retro-shear zone, gradual ↓T, ↓P in its HW	n.a.	Steep flattening to reverse shearing. Reverse shear strain ↑ → retro-shear zone	U-shape younger → interior of orogen	↓T/↓P in HW of retro-shear zone coeval with ↑T/↑P in FW	Reverse > normal (no extension)
Jamieson et al. (1998) Thermomechanical models CE and CF	Exhumed HT retro-shear zone	IT-B, IT-D to C-D	Sharp in the FW of the retro-shear zone, gradual ↓T, ↓P in its HW	Variable 450–700 °C 600–1300 MPa	Steep flattening to reverse shearing. Reverse shear strain ↑ → retro-shear zone	Younger → retro-shear zone	↓T/↓P on prowedge side coeval with ↑T/↑P on retrowedge side	Reverse > normal (no extension)
Willett (1999a) Thermomechanical erosion effect	Synform ± antiforms of various geometries in HW of retro-shear zone Various amount of exhumation	n.a.	Sharp (gradual in 1 model) in the FW of the retro-shear zone, gradual ↓T, ↓P in its HW	n.a.	Steep flattening to reverse shearing. Reverse shear strain ↑ → retro-shear zone	Younger → deeper structural levels	n.a.	Reverse > normal (no extension)
Bonnet et al. (2008) Analogue erosion effect	Foreland fold-and-thrust belt to suprastructure klippe to domal culmination of midcrustal nappe stack	n.a.	n.a.	n.a.	Reverse shearing throughout	Younger → deeper structural levels	↓P on prowedge side coeval with ↑P on retrowedge side	Reverse > normal (no extension even when no erosion)
Channel flow								
Jamieson et al. (2002) Model HT-6	Top of channel exhumed; progressive gradient to suprastructure	H-B, C-D	Progressive ↑T → center of the channel	600–750 °C 800–1200 MPa	Normal to reverse shearing from the roof to the base of the channel overprinted by flattening	n.a.	Not defined, but ↓T/↓P coeval with ↑T/↑P	Reverse = normal for bounding shear zones
Jamieson et al. (2004) Model HT1	Exhumed small channel surrounded by suprastructure	H-B to IB-H IT-D to C-D	Progressive ↓T/↓P → top of channel Sharp ↓T/↓P in FW of channel (inverted gradient)	400–800 °C 300–1000 MPa	Normal to reverse shearing from the roof to the base of the channel overprinted by flattening	Uniform in channel and FW	↓T/↓P in channel coeval with ↑T/↑P in its FW	Reverse = normal for bounding shear zones
Jamieson et al. (2006) Model HT111	Foreland fold-and-thrust belt to exhumed channel to suprastructure klippe to hinterland dome cored by migmatites and a hot fold nappe	H-B to IB-H IT-D	n.a.	700–850 °C 700–1300 MPa	Normal to reverse shearing from the roof to the base of the channel overprinted by flattening Decreasing strain gradient toward lower structural level of the dome	Younger from front to rear of the channel	↓T/↓P in channel coeval with ↑T/↑P in its FW	Reverse = normal for bounding shear zones
Jamieson et al. (2007) Model EGO-1 Hot fold nappes	Foreland fold-and-thrust belt to hot fold nappes still 10 km below the surface	H-B to IB-H IT-D to C-D	HP fold nappes above LT-MP rocks To stack of HT-MP fold nappes	500–900 °C 1000–1850 MPa	Reverse throughout Recumbent fold nappes interspersed with suprastructure synclines and anticlines	n.a.	Variable but ↓T/↓P coeval with ↑T/↑P in places	Reverse > normal (no extension)

Note: Abbreviations: MCC—metamorphic core complex; H—high; M—medium; L—low; IT—isothermal; IB—isobaric; C—cooling; H—heating; D—decompression; → —toward; ↑—increase; ↓—decrease; T—temperature; P—pressure; HW—hanging wall; FW—footwall.

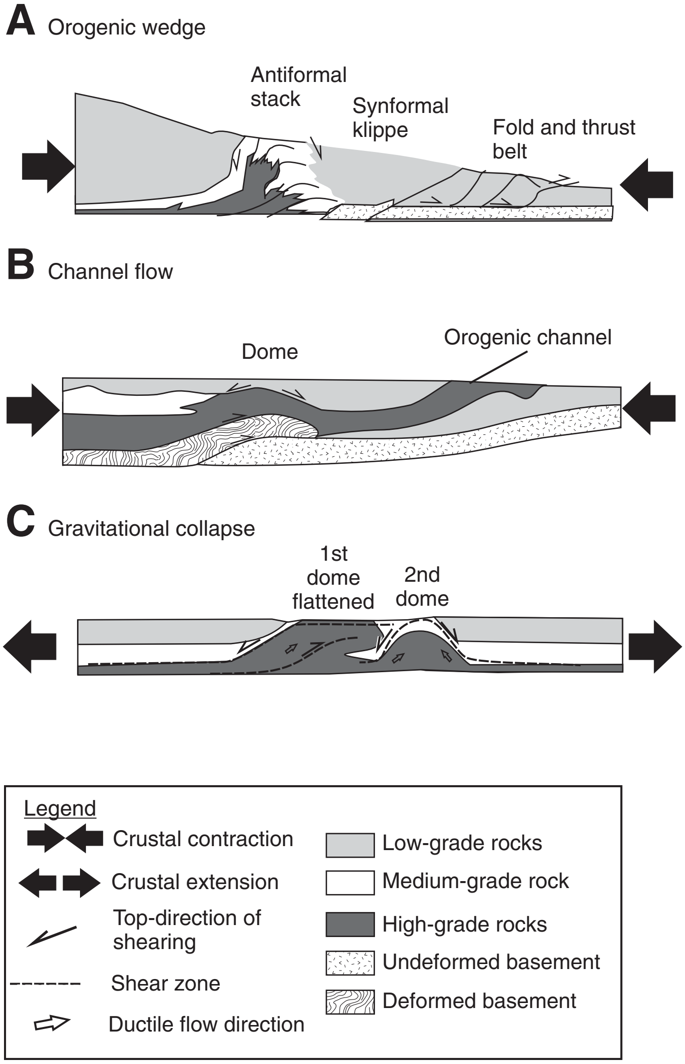

D

Spatial distribution of finite strain patterns	Metamorphic field gradient	Spatial distribution of cooling ages	Spatial distribution of *P-T-t* paths
Reverse shearing and steep flattening	Gradual in hanging wall Sharp in footwall of retro-shear zone	Important gradient in all thermochrono-meters: younger toward deeper structural levels. Variable geometry.	Exhumation at higher structural levels coeval with burial at deeper structural levels
Coeval normal and reverse shearing at the roof and base of the channel, respectively	Sharp in footwall of the channel Gradual to sharp in the hanging wall of the channel	Lateral gradient: younger toward the front of the channel Uniform cooling at any given longitudinal section of the channel	Broadly synchronous exhumation throughout the channel coeval with burial of footwall rocks Protracted residence time in the middle crust
Prevalence of horizontal flattening Outward verging shear zones at dome margins	Sharp at supra-infra-structure contact	Model-dependent	Exhumation paths only, variable timing

Figure 2. Test for the three main modes of exhumation in collisional orogens. The model from each mode that is most consistent with the overall geometry of the area surrounding the Monashee Complex in the southeastern Canadian Cordillera (cross section in Fig. 3A) is illustrated as a sketch redrawn from the original publication. (A) Progressive underthrusting model with décollements and erosion (modified from Fig. 2C-3 *in* Malavieille, 2010). (B) Channel-flow model HT111 (Jamieson et al., 2006). (C) Type 2 sequential core complex model (Fig. 5D *in* Tirel et al., 2009). Models are not to scale. (D) Set of diagnostic criteria for each mode of exhumation. The criteria apply to all models from a given mode, not only the models illustrated in A–C. See text for detail.

and the wedge maintains its critical taper by thickening and growing laterally (Willet, 1999a; Vanderhaeghe et al., 2003a). Erosion significantly modifies the wedge dynamics by inducing a continuous cycling of rock that promotes significant exhumation of midcrustal rocks. The wide range of possible parameters produces a similarly wide range of dynamics, but some characteristics are common to most wedges with active erosion. In the vast majority of models, rocks enter the wedge from the proside, are buried and heated, and then follow an exhumation path in the hanging wall of the retro-shear zone, which migrates retroward during the lateral growth of the wedge (Willett et al., 1993; Jamieson et al., 1998; Batt and Braun, 1999; Willett, 1999a; Jamieson et al., 2002). This cycle results in the general key characteristics listed in Figure 2A. Finally, numerical and analogue models demonstrate that extension is unlikely in orogenic wedges (Willett, 1999b; Vanderhaeghe et al., 2003b; Bonnet et al., 2008). Therefore, major normal faults (or shear zones) should be younger and not related to the formation of an orogenic wedge.

In this mode of exhumation, it is the progressive underthrusting analogue model with décollements and erosion that is most consistent with the overall geometry of the southeastern Canadian Cordillera (Fig. 2A; Malavieille, 2010). In this model, exhumation results from the combined effect of underplating at the base of the wedge and denudation at the surface, which give rise to an antiformal stack of duplexes surrounded by low-grade rocks. In contrast to most other orogenic wedge models, a normal-sense shear zone may develop by vertical shearing of the left side of the first (top) duplex as it is uplifted.

Wedge dynamics have been shown to prevail until a significant thickness of the lower crust reaches a critical viscosity below which it can no longer support the weight of the wedge (Vanderhaeghe et al., 2003a). From this point onward, the dynamics of the orogen are not controlled by the critical-taper theory, but rather by the channel-flow concept derived from fluid mechanics (Grujic, 2006). Driven by the pressure gradient between a thick orogenic core and a thin foreland, a Poiseuille-dominated flow can be produced in large, hot, orogen-scale thermomechanical models that

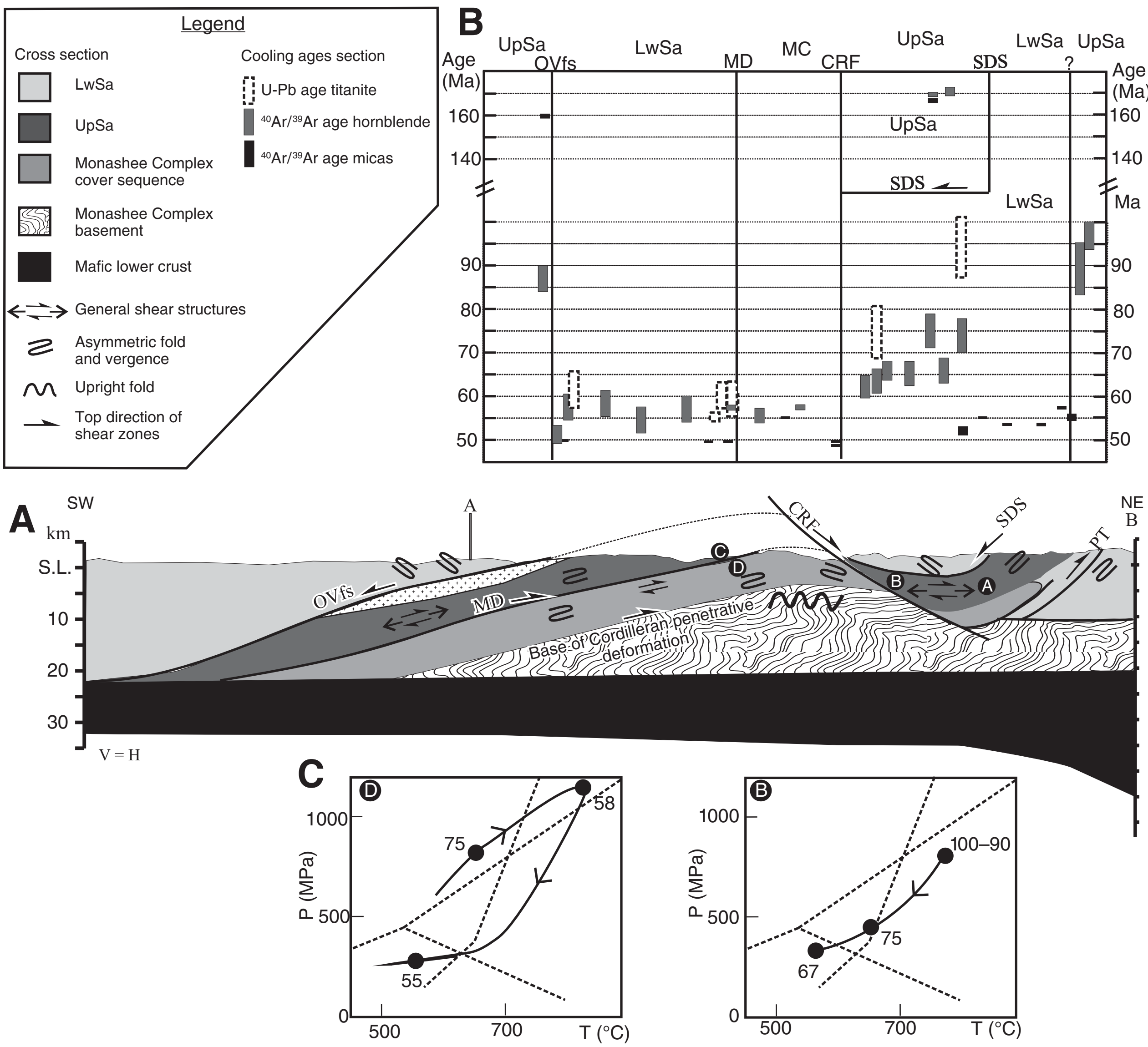

Figure 3. Geological cross section with summary of structural, metamorphic, and thermochronologic data. (A) Geological cross section (modified from Gibson et al., 2005) and finite strain patterns. Legend and abbreviations are the same as for Figure 1B except for: (1) the black fill, which represents a mafic lower crust indicated by seismic-refraction profiles (cf. Burianyk and Kanasewich, 1995); and (2) the basement of the Monashee Complex (MC) (folded pattern), which only includes rocks that have escaped Cordilleran tectonism (Gervais et al., 2010), whereas on the map of Figure 1B, basement refers to lithologic units irrespective of their timing of deformation. The trace of the cross section is shown in Figure 1B. (B) Thermochronologic data projected onto cross-section A–B. (C) Pressure-temperature-time (*P-T-t*) paths for the location D of the Monashee Complex (constructed from data published in Crowley and Parrish, 1999; Foster et al., 2004) and for location B of the lower Selkirk allochthon (modified from Scammell, 1993). Abbreviations: LwSa—Lower Selkirk allochthon; UpSa—Upper Selkirk allochthon; OVfs—Okanagan Valley fault system; CRF—Columbia River fault; SDS—Selkirk Detachment System; MD—Monashee décollement; S.L.—sea level.

incorporate a stepwise decrease in viscosity at high temperature to simulate partial melting (Fig. 2B; Beaumont et al., 2001; Jamieson et al., 2002, 2004, 2006; Beaumont et al., 2004, 2006). In these models, significant exhumation occurs only when active erosion at the mountain front leads to an upward bifurcation of the channel, which then flows toward the erosion front. Alternatively, underthrusting of a stiff indentor can expel overlying low-viscosity rocks, which are exhumed by the equivalent of the indentor thickness (Jamieson et al., 2007, 2010). In addition, underthrusting of an indentor beneath a flowing channel (Fig. 2B) promotes exhumation, first by doming the channel and inducing extension of the overlying upper crust (Beaumont et al., 2004), and then by squeezing out this early-formed dome above the indentor (Jamieson et al., 2006, 2007). In contrast to the other exhumation modes, the progressive exhumation of the channel leads to a lateral—rather than vertical—spatial gradient of cooling ages, which become older toward the rear of the channel (Fig. 2B). The other general key characteristics of this model are listed in Figure 2B.

In the channel-flow category, it is the HT111 model of Jamieson et al. (2006) that is most consistent with the overall geometry of the southeastern Canadian Cordillera (Fig. 2B). In this model, a dome forms by the underthrusting of a stiff basement indentor beneath a flowing midcrustal channel. Once thermally softened, the tip of the indentor is thrust back over the rear of the indentor.

Gravitational collapse of the thickened welt takes place when the convergence rate declines to a point at which the related traction force can no longer sustain the weight of the thickened orogen. Three main modes of gravitational collapse of thickened orogens can lead to the exhumation of midcrustal rocks (Rey et al., 2001). If the middle crust is stiff and refractory, extension would result in the formation of crustal-scale boudins cored by competent rocks such as older basement. This is akin to the heterogeneous crustal boudinage model proposed by Price and Monger (2003) for the formation of the domes of the southeastern Canadian Cordillera. On the contrary, a low-viscosity middle crust would flow. In the models considered herein, those with a precursor zone of weakness, such as upper-crustal faults or midcrustal magmatic sills, result in the formation of metamorphic core complexes formed by the flow of the ductile crust toward a necked upper crust (Tirel et al., 2006, 2009; Brun et al., 1994; Rey et al., 2009). Alternatively, models without such weaknesses result in proward midcrustal flow that induces thrusting in the foreland (Jamieson et al., 2002, 2010; Beaumont et al., 2010). Despite important differences, all these models share common characteristics (Fig. 2C). In general, reverse shear zones, which contributed to the thickening phase, should be older than the normal shear zones, which exhumed the complex. Better distinctive criteria predicted by this model are listed in Figure 2C. In the gravitational collapse category, it is the type 2, sequential core complex model (fig. 5D *in* Tirel et al., 2009) that is most consistent with the overall geometry of the southeastern Canadian Cordillera.

In this model, the ductile middle crust flows toward the necked upper crust to form a first asymmetric dome that is then flattened as a second dome develops in its footwall. The early-formed dome is bounded by reverse and normal shear zones at its base and roof, respectively. This is one of the rare models of this exhumation mode resulting in coeval oppositely verging shear zones.

TECTONIC SETTING

The ~900-km-wide southern Canadian Cordillera can be subdivided into five morphogeological belts (Fig. 1A) that record a protracted tectonic history from the Early Jurassic to the Eocene (e.g., Evenchick et al., 2007). The Insular, Intermontane, and Foreland belts consist of rocks of mainly low metamorphic grade, whereas the Coast and Omineca belts consist of variously deformed metamorphic and plutonic rocks (Monger et al., 1982). The study area is located within the southern part of the Omineca belt (Fig. 1A).

Four main periods led to the formation of the Omineca belt (Evenchick et al., 2007): the Jurassic, 145–135 Ma, 115–90 Ma, and 74–59 Ma. The Jurassic was a period of final amalgamation of terranes that were thrust and obducted over North American pericratonic terranes and basement. The southwest-vergent deformation and exhumation that characterized the Jurassic (Colpron et al., 1996) was interpreted to have developed in a prowedge setting (Brown and Willett, 1993; Gibson et al., 2005). The two mid-Cretaceous periods involved thickening and regional uplift accompanied by the formation of zones of penetrative northeast-verging deformation at midcrustal levels (Evenchick et al., 2007). The Late Cretaceous period (74–59 Ma) is critical for this study because it is during this period that ~200 of the ~250 km of net shortening took place in the Foreland belt at this latitude (Price and Sears, 2000). It is commonly accepted that the Paleogene (60–48 Ma) was a period of extension and gravitational collapse of the thickened orogenic welt (e.g., Coney and Harms, 1984; Parrish et al., 1988; Liu, 2001; Teyssier et al., 2005), a view partially contested by the results of this study and that of Gervais et al. (2010).

ARCHITECTURE OF THE SOUTHEASTERN CANADIAN CORDILLERA

In order to critically test the three modes of exhumation (Fig. 2) and to improve the subdivision scheme of the southeastern Canadian Cordillera, we compiled plutonic, structural, metamorphic, and geochronologic data from 52 published papers and unpublished theses (Table 2). The striking differences in terms of names and spatial distribution of tectonometamorphic units on regional maps published in the past 10–15 yr (cf. Parrish, 1995; Colpron et al., 1999; Teyssier et al., 2005; Brown and Gibson, 2006; Carr and Simony, 2006; Glombick et al., 2006a; Johnson, 2006) motivated us to propose an updated subdivision scheme. We build on Read and Brown (1981), who divided the crust of the southern Omineca belt into two main units: the Selkirk allochthon and the Monashee Complex. The Selkirk allochthon includes variously deformed and metamorphosed rocks from accreted terranes, as well as sediments and mafic sills deposited/intruded on the attenuated western margin of the North American craton. It was thrust onto basement rocks of the craton and its cover sequence, which together form the Monashee Complex. These two units are clearly distinguished by the timing of their respective plutonic events. The Selkirk allochthon is composed of various plutonic suites of Devonian–Mississippian, Jurassic, Early to Late Cretaceous, and Paleogene ages, whereas the underlying Monashee Complex contains only Paleoproterozoic (in the basement) and Paleogene intrusions (Table 2). Notwithstanding their distinct lithostratigraphic origins and tectonometamorphic histories (see following), their contrasting plutonic histories alone imply that the two units were not juxtaposed until the Late Cretaceous, at the earliest, and cannot be grouped into one unit, as has been done recently (e.g., Vanderhaeghe et al., 1999; Williams and Jiang, 2005; Teyssier et al., 2005; Glombick et al., 2006a). Our compilation further suggests that the Selkirk allochthon should be divided into an upper and a lower panel because they each have contrasting structural, metamorphic, and geochronologic characteristics. The upper Selkirk allochthon consists of greenschist- to lower-amphibolite–facies rocks deformed by SW-verging folds in the Jurassic, whereas the lower Selkirk allochthon consists of upper-amphibolite–facies rocks that were strongly deformed by top-to-the-E/NE shearing for a protracted period in the Cretaceous to Paleocene (Table 2). The new subdivision is presented on a map (Fig. 1B) and on a cross section (Fig. 3A). The reader is referred to Gervais (2009) for an extensive discussion about the locations of the boundaries and other specific information concerning this subdivision scheme. The architecture of the exposed crustal section thus consists of a stack of three tectonometamorphic units, similar to the three crustal zones of Carr (1991).

SPATIAL DISTRIBUTION OF FINITE STRAIN PATTERNS AND METAMORPHIC FIELD GRADIENTS

This section describes the salient structural, metamorphic, and geochronologic characteristics of each tectonometamorphic unit from lower to upper structural levels. The spatial distribution of finite strain pattern and metamorphic field gradients derived from this description will be used to test the tectonic models of exhumation. The sources of data and related references are given in Table 2, unless otherwise cited.

Monashee Complex

The deepest unit is the Monashee Complex, which consists of two domes, Frenchman Cap in the north and Thor-Odin in the south (Fig. 1B). On its east flank, the Monashee Complex is bounded by the east-dipping Columbia River fault, a brittle-ductile normal fault that was active between

TABLE 2. COMPILATION OF IGNEOUS, STRUCTURAL, METAMORPHIC, AND GEOCHRONOLOGIC DATA FOR THE SOUTHEASTERN CANADIAN CORDILLERA AT THE LATITUDE OF THE MONASHEE COMPLEX

		Timing of intrusions	Structure*	Timing (Ma) of transposition foliation (S_T)†	Peak *P-T*	Timing of peak *P-T* (Ma)§	Retrograde *P-T*	Timing of cooling# (Ma)
Cross-section A-B	UpSa	Devonian–Mississippian Jurassic Cretaceous Paleogene[15]	SW-verging folds[3,25,26] NE-verging in NE area[24,27] L_S: variably developed from NW-SE[34] to E-W[26]	167 < S_T < 156[3] 154 < S_T < 125[25]	600–800 MPa 550–650 °C[25,26]	~148 Mnz[25] ~135 Mnz[24]	Sil overprintat SDS (ca. 92 Ma)[3]	Cariboo Mtn.: 140–129 Bt[25] N. Monashee Mtn: 87, 97 Hbl[48] 57–54 Bt[48]
	LwSa	Devonian–Mississippian Jurassic Cretaceous Paleogene[1,2,3,15]	Top-to-E shearing[1,2,4,28] Top-to-SW at SDS[3] L_S: pervasive WNW-ESE to W[1]	NE of A: S_T >90[3] 64 < S_T < 58[4] A: 122 < S_T < 63[4] ~104 < S_T < 100[2,3] B: 135 ≥ S_T < 71[1] C: 97 < S_T < 57[1]	NE of A: 720 MPa at 680 °C[39] A-B: 650–800 MPa 700–750 °C[1]	NE of A: 84–70 and 65–58[3,4,29] A-B: 100–90[1–4] C: 132, 120–110, 86–81, 65[6]	A-B: 350–550 MPa at 550–650 °C[1]	NE of A: 57–53 Bt[32] A: 98–91 Tnt[1] 75–66 Hbl[1] ~52 Ms[1] B: 74 Tnt[1] 70–64 Hbl[1] 53 Rt
	MC	Proterozoic Paleogene[6,16,17]	Top-to-E shearing[9,14, 30] L_s: pervasive W[9,14, 30] No penetrative Cordilleran foliation in the core[51]	S_T > 55[6]	900–1100 MPa 750–800 °C[13,33]	63–56[6,13,30]	Sil + And overprint[12,14,30,31,33]	
Section Revelstoke-Sicamous	UpSa	Devonian–Mississippian Jurassic Cretaceous Paleogene[15]	SW-verging folds [9,36] L_S: variably developed, variably oriented[9,35]	East: 173 < S_T < 168[36]	East: 500–700 MPa 450–600 °C[36,38]	East: 173–168[36]	East: 300–500 MPa at ~450–550 °C[36,38]	East: 171–168 Hbl[36] 156–131 Bt[36] West: 111–74 Hbl[9] 67 Ap[37]
	LwSa	Devonian–Mississippian Jurassic Cretaceous Paleogene[1,6,9,15]	Top-to-E shearing[1,2,14] L_s: pervasive W[1,14] Top-to-W at OVfs[9]	MD: 92, 67 < S_T < 58[6,9] OVfs: 70 < S_T < 56[9]	750–900 MPa 720–800 °C[49]	MD: 100–70[9,23,43] OVFS: 160–155 100–57[43]	?	58–54,51 Hbl[9]
	MC	Proterozoic Paleogene[6,16,17]	Top-to-NE shearing[12,14,33] L_s: pervasive W[14,33] No penetrative Cordilleran foliation in the core[51]	Upper level: 58 < S_T < 56[17] Lower level: 52 < S_T < 49[17]	Upper level: 900–1100 MPa 750–800 °C[33] Lower level: Sil-Kfs[14,33]	Upper level: ca. 58[12,17] Lower level: 52–49[12]	~200–440 MPa at 550–650 °C[33]	Upper level: 55 Hbl[12] 49 Bt[12] Core: Paleoproterozoic and 49 Tnt[12,51]
Section Vernon-Nakusp	UpSa	Triassic Jurassic Cretaceous Paleogene[9,11,18]	Upright to SW-verging folds [9,40,41] L_S: variably developed, variably oriented[9,40,41]	East and West: 171 < S_T < 162[6,11]	West: Greenschist[10,11,41] East: 600–800 MPa ~520–600 °C[40]	171–162[6]	n.a.	160 Bt[10]
	LwSa	Devonian–Mississippian Cretaceous Paleogene[9,11,15]	Top-to-E shearing L_s: pervasive WNW-ESE to WSW-ENE[8–11,18–20] Top-to-W at OVfs[8–11]	MD: 62 < S_T < 58[22] OVfs: 102 < S_T < 47[9,11]	700–1000 MPa 750–850 °C[7] 600–900 MPa 640–775 °C[8]	MD: 62–55[42] OVFS: 155–143 92–86 66–56[11]	?	MD: 62–55 Tnt[42] 59–54 Hbl[44,52] 48 Bt[52] OVFS: ~62 Tnt[11] 52–48 Hbl + Bt[10,52]
	MC	Proterozoic Paleogene[15,19–23]	Top-to-NE shearing[19,21,50] L_s: pervasive[45] WSW-ENE[19,44,50]	56 < S_T < 51[19,21]	800–1000 MPa 725–850 °C[47]	65–54[23] 60–56[20,21] 61–52[46]	400–500 MPa 700–800 °C[47]	n.a.

Note: The areas encompassed by the locations with respect to the Frenchman Cap Dome (FCD) are shown on Figure 2. Letters refer to locations on the map of Figure 2. Mineral abbreviations are after Kretz (1983). Abbreviations: OVfs—Okanagan Valley fault system; MD—Monashee décollement; SDS—Selkirk Detachment System. References: 1—Scammell (1993); 2—Sevigny et al. (1990); 3—Gibson et al. (2004, 2005, 2008); 4—Crowley et al. (2003); 5—this study; 6—Parrish (1995); 7—Glombick (2005); 8—Teyssier et al. (2005); 9—Johnson (1994); 10—Bardoux (1993); 11—Glombick et al. (2006b); 12—Crowley and Parrish (1999); 13—Foster et al. (2004); 14—Journeay (1986); 15—Wheeler and McFeely (1991); 16—Crowley (1999); 17—Crowley et al. (2001); 18—Carr (1991); 19—Johnston et al. (2000); 20—Vanderhaeghe et al. (1999); 21—Hinchey et al. (2006); 22—Carr (1992); 23—Kuiper (2003); 24—Currie (1988); 25—Reid (2002); 26—Marchildon (1999); 27—Simony et al. (1980); 28—Raeside and Simony (1983); 29—Digel et al. (1998); 30—Gibson et al. (1999); 31—Scammel (1986); 32—Ghent and Villeneuve (2006); 33—Gervais and Brown (2007); 34—Murphy (1987); 35—Colpron (1997); 36—Colpron et al. (1996); 37—Lorencak et al. (2001); 38—Crowley et al. (1996); 39—Tinkham and Ghent (2005); 40—Lemieux (2006); 41—Unterschutz (2002); 42—Carr (1995); 43—Gilley (1999); 44—Spark (2001); 45—Williams and Jiang (2005); 46—Hinchey et al. (2007); 47—Norlander et al. (2002); 48—Boggs (2004); 49—Nyman et al. (1995); 50—Kruse (2007); 51—Gervais et al. (2010); 52—Vanderhaeghe et al. (2003b).

*L_s—stretching and mineral lineation.

†Based on the U-Pb age of crosscutting intrusions.

§Based on the U-Pb age of monazite in schist or zircon in leucosome.

#Based on $^{40}Ar/^{39}Ar$ plateau ages for hornblende, biotite, and muscovite and U-Pb age for titanite.

49 and 47 Ma (Mulch et al., 2006). On its west flank, it is bounded by the westerly dipping, Monashee décollement (Brown et al., 1992; McNicoll and Brown, 1995), a major ductile reverse shear zone. Recent studies in the Frenchman Cap dome (Crowley et al., 2008; Gervais et al., 2010) revealed a stepwise disappearance of pervasive Cordilleran deformation downward, with a 4–5-km-thick section of felsic basement gneisses preserving a Paleoproterozoic migmatitic gneissosity, and with Cordilleran deformation limited to local upright folds and meter-scale shear zones. Above this orogenic base, an ~5-km-thick rock package records high finite general shear-strain characterized by a transposition foliation and a well-developed W-plunging lineation (stretching and mineral), toward which minor fold axes have been rotated into near parallelism during top-to-the-E shearing. Peak metamorphic assemblages in metapelites reached the kyanite–K-feldspar field and were heterogeneously retrogressed in the sillimanite and andalusite fields. Ductile deformation and high-temperature metamorphism took place between 63 and 49 Ma, depending on structural level. Gervais et al. (2010) showed that the dome formed between 52 and 49 Ma synchronously with the waning stages of top-to-the-E crustal shearing and shortly after the underthrusting of a basement ramp.

Similar structural and metamorphic features were documented in the southern Thor-Odin dome. Top-to-the-NE noncoaxial finite strain is ubiquitous, and near parallelism between WSW-ENE–stretching lineations and minor fold axes is also common. Peak metamorphic conditions reached conditions similar to those of the Frenchman Cap dome, but more melt was produced as a result of crossing the low-pressure biotite breakdown reaction, which produces cordierite and garnet as peritectic products (Norlander et al., 2002). The timing of top-to-the-NE shearing and high-temperature metamorphism is also the same as that of the Frenchman Cap dome and occurred between 56 and 51 Ma. The main difference between the two domes is that the base of Cordilleran strain has not been identified in the Thor-Odin dome and that a body of Cordilleran diatexite with a subvertical lineation and a dome-up sense of shear was mapped (Vanderhaeghe et al., 1999). The presence of this diatexite body, combined with the isothermal decompression path documented nearby, constituted the basic arguments in favor of the widely publicized model of doming by vertical flow (Vanderhaeghe and Teyssier, 1997; Vanderhaeghe et al., 1999; Norlander et al., 2002; Teyssier and Whitney, 2002; Whitney et al., 2004; Teyssier et al., 2005). However, the absence of a Cordilleran penetrative fabric in the core of the Frenchman Cap dome combined with the continuity of lithologic markers across the domes (Read, 1980) rule out the vertical-flow model for the formation of the domes of the Monashee Complex (Gervais et al., 2010).

Lower Selkirk Allochthon

Overlying the Monashee Complex, there is the 8–10-km-thick lower Selkirk allochthon. All features described here are common to the continuous exposure of the lower Selkirk allochthon from the western flank of the Monashee Complex to the northern Monashee Mountains, where isograds and lithological contacts are continuous toward the SE in the Selkirk Mountains (Fig. 1B). Along cross-section A–B (Fig. 3A), the panel is exposed in the footwall of the top-to-the-W Okanagan Valley fault system (OVfs; as per Johnson, 2006) to the west of the Monashee Complex; it is domed above the complex, down-faulted under the surface by the Columbia River fault to the east of the complex, and surfaces again in the footwall of the Selkirk detachment system in the Selkirk Mountains. As suggested by Brown and Gibson (2006), the Okanagan Valley fault system and the Selkirk detachment system likely formed a single structure before being cut by the Columbia River fault.

The lower Selkirk allochthon is characterized by high finite general shear-strain like the upper part of the Monashee Complex. It has a transposition foliation dipping shallowly to the W-SW and a pervasive E-W to WSW-ENE stretching lineation, toward which minor fold axes have been substantially rotated during top-to-the-E shearing. Because such rotation by noncoaxial shearing alone requires a very high amount of strain, Scammell (1993) concluded that deformation possessed a component of coaxial strain (i.e., general shear). The mixture of noncoaxial and coaxial structures observed in the structural center of the lower Selkirk allochthon supports this conclusion (Journeay, 1986; Scammell, 1993; Johnson, 1994; Glombick, 2005). In the southern part of the map (Fig. 1B), the lower Selkirk allochthon is bounded at its roof by the top-to-the-W Okanagan Valley fault system, and at its base by the top-to-the-E/NE Monashee décollement. These two oppositely verging shear zones are several hundreds of meters thick and consist of mylonite intruded by large volumes of sheared leucogranite (Journeay, 1986; Scammell, 1993; Johnson, 1994; Glombick et al., 2006a). In the northern part of the map (Fig. 1B), the boundary between the lower Selkirk allochthon and the upper Selkirk allochthon was mapped as a gradational, SW-dipping metamorphic gradient (Simony et al., 1980; Raeside and Simony, 1983). In contrast to the southern part of the map, the lower Selkirk allochthon is therefore not bounded by a normal shear zone in the northern part of the study area (Fig. 1B).

The lower Selkirk allochthon is at the upper amphibolite facies. Rocks are highly migmatitic and intruded by leucogranite sills, dikes, and plutons that together form between 30% and 60% of any outcrop (Journeay, 1986; Carr, 1991; Scammell, 1993; Glombick et al., 2006a; Johnson, 2006). Metapelitic schists contain sillimanite and K-feldspar, except near the boundaries with the upper Selkirk allochthon, where muscovite is commonly stable (Fig. 1B). At the latitude of the Thor-Odin dome, the muscovite-out and the kyanite-out isograds are exposed within an attenuated gradient less than ~3 km thick in the footwall of the Okanagan Valley fault system (Carr, 1991; Bardoux, 1993; Lemieux, 2006; Glombick et al., 2006a), whereas in the northern Monashee and Selkirk Mountains, these two isograds are also exposed, but within a thickness in excess of 7 km structurally above the upper Selkirk allochthon–lower Selkirk allochthon boundary (Simony et al., 1980; Raeside and Simony, 1983; Digel et al., 1998).

A key characteristic of the lower Selkirk allochthon is a protracted history of high-temperature metamorphism and deformation. The emplacement of numerous synkinematic leucogranites between 105 and 90 Ma throughout the lower Selkirk allochthon implies that it was deforming at high temperature at this time (Scammell, 1993; Johnson, 1994; Parrish, 1995; Crowley et al., 2003), but crosscutting relationships of other leucogranite dikes further suggest that a substantial amount of strain was produced before ca. 135 Ma in the northern part of the area (between A and B in Fig. 1B; Scammell, 1993) and after 70 Ma in the southern part of the area. Furthermore, a major thermal event near area A (Fig. 1B) between 105 and 90 Ma is indicated by the cluster of monazite dates in migmatitic schists and of zircon ages in leucogranite. The temperature was also high enough for protracted growth of zircon in leucosomes in the Early Cretaceous and from 120 to 65 Ma in the hanging wall of the Monashee décollement near area C (Fig. 1B), and in the Jurassic and from 100 to 57 Ma in the footwall of the Okanagan Valley fault system near Sicamous and Vernon (Fig. 1B). These observations suggest that the thermal peak was reached in the mid-Cretaceous throughout, but that the temperature remained high until the Paleocene in lower Selkirk allochthon rocks cropping out west of the Monashee Complex.

Upper Selkirk Allochthon

The upper Selkirk allochthon includes all rocks deformed and metamorphosed prior to ca. 120 Ma. Most of these rocks are at the garnet grade or lower, but local areas reached the sillimanite-muscovite grade

(Fig. 1B). Except for rocks west of Blue River (Fig. 1B), sillimanite is post-tectonic and occurs in pluton aureoles or in the hanging wall of the Selkirk detachment system (Fig. 1B). Similarly, most of the upper Selkirk allochthon was deformed by W- to SW-vergent Jurassic folds, but it locally records NE-vergent Jurassic structures, mostly in the NE part of the area shown in Figure 1B. These rocks cooled below the hornblende and mica closure temperature (350–550 °C) before ca. 120 Ma, except near the lower Selkirk allochthon–upper Selkirk allochthon boundary, where Late Cretaceous ages are recorded (Fig. 3B). Consequently, rocks of the upper Selkirk allochthon had been exhumed above the brittle-ductile transition (300–400 °C) by the mid-Cretaceous and thus formed the upper-crustal lid of the southeastern Canadian Cordillera in the Late Cretaceous to Paleogene.

SPATIAL DISTRIBUTION OF COOLING AGES

Several studies have documented the distribution of cooling ages throughout the lower Selkirk allochthon. In our compilation (Table 2; Fig. 3B), we retained the original authors' interpretations of U-Pb dates, but only retained $^{40}Ar/^{39}Ar$ hornblende, biotite, and muscovite plateau ages derived from >80% of the released ^{39}Ar gas to avoid problems associated with excess argon and complex cooling/reheating histories. Several interesting features are derived from Figure 3B, which shows all cooling ages of the lower Selkirk allochthon projected onto cross-section A–B. First, it highlights the contrast between the upper Selkirk allochthon, which records mainly Jurassic ages, and the lower Selkirk allochthon, which records ages varying between 95 and 55 Ma. Rocks of the upper Selkirk allochthon located near the contact of the lower Selkirk allochthon, however, record younger hornblende Ar/Ar ages in the range 89–110 Ma, which coincide with the thermal peak recorded in the lower Selkirk allochthon (Table 2). Second, there is a trend of titanite and hornblende cooling ages that become younger southwestward in lower Selkirk allochthon rocks cropping out NE of the Monashee Complex (Figs. 3A and 3B), but not in those cropping out west of the complex. Titanite ages decrease from 90–98 Ma at location A (Fig. 1B) to ca. 74 Ma at location B, to ca. 62 Ma at location C (see Table 2 and following section for data) and are then constant at 62–55 Ma throughout the lower Selkirk allochthon west of the Monashee Complex. Similarly, hornblende cooling ages decrease from ca. 75 to ca. 62 Ma between locations A and B, and are then constant at 57–54 Ma throughout the lower Selkirk allochthon west of the Monashee Complex. As noted earlier, this trend is also reflected in U-Pb zircon ages from leucosomes that range in age between 100 and 90 Ma NE of the Monashee Complex, whereas those west of the complex extend to ages as young as ca. 57 Ma. Third, mica cooling ages are slightly younger NE of the Monashee Complex, where they range between 56 and 53 Ma, than west of it, where they cluster at 50–47 Ma. Consequently, there is no clear trend of cooling ages across structural levels of the lower Selkirk allochthon (as proposed by Parrish, 1995), but there is a lateral NE-SW trend. Because this trend is perpendicular to the axis of the autochthonous basement of the Monashee Complex (Armstrong et al., 1991; Crowley et al., 2001; Gervais et al., 2010), it implies that rocks of the lower Selkirk allochthon that were thrust above the complex cooled prior to rocks that were not.

PRESSURE-TEMPERATURE-TIME PATHS

In this section, *P-T-t* paths are presented for different localities of the lower Selkirk allochthon and of the Monashee Complex. Robust paths are available for the lower Selkirk allochthon NE of the Monashee Complex (locations A and B in Fig. 1B) and from the Frenchman Cap and Thor-Odin domes in the complex itself. However, no such path is available for the lower Selkirk allochthon west of the complex (Table 2).

New Results from the Monashee Décollement

Two samples, less than 20 m apart, were collected at area C (Fig. 1B) to construct a P-T-t-deformation (*P-T-t-d*) path. Rocks at this locality consist of interlayered semipelitic schists, quartzofeldspathic gneisses, and boudinaged amphibolitic layers. As for all rocks of the ~1-km-thick Monashee décollement, they are migmatitic, mylonitic, and record top-to-the-E sense of shear in a variety of kinematic indicators (Fig. 4). Many observations indicate that melt was present during deformation (e.g., Fig. 4C). Migmatitic schists contain more than 40% of leucocratic material in the form of leucosome (15%–30%) and leucogranite intrusions (25%–40%). The minimum age of deformation is provided by the 57.0 ± 0.2 Ma age of a suite of leucogranite that crosscuts the mylonitic foliation at right angles (Scammell, 1993).

Thermobarometry for Migmatitic Pelitic Schist Sample Fg-462a

Sample Fg-462a is one of the rare pelitic schist of this locality. It is migmatitic and contains the assemblage rutile-garnet-ilmenite-sillimanite–K-feldspar–biotite. Prismatic and fibrolitic sillimanite is present in the matrix and is concentrated around resorbed garnet porphyroblasts, whereas no relict kyanite was observed. Garnet comprises only 3%–5% of the modal mineral assemblage and commonly shows preferential resorption of sigmoidal tails indicative of top-to-the-E sense of shear (Fig. 5A). The metamorphic paragenesis in these sigmoidal tails, which consists of sillimanite, biotite, ilmenite, plagioclase, and quartz (Fig. 5A), implies peak metamorphic conditions in the sillimanite field above the muscovite-dehydration reaction, but below the upper thermal stability of biotite (stippled area in Fig. 6). Garnet cores exhibit little compositional zoning, with X_{sps} = 0.04–0.06, X_{grs} = 0.04–0.05, X_{pyr} = 0.21–0.24, and Fe/(Fe + Mg) = 0.74–0.77 (Table 3), but margins show an increase in X_{sps} (0.09–0.17), and an increase in Fe/(Fe + Mg) = 0.79–0.85. Such compositional spikes at resorbed garnet margins are commonly interpreted as evidence for garnet breakdown in the presence of melt by the retrograde reaction (Spear et al., 1999; Kohn and Spear, 2000):

$$\text{Grt} + \text{Liq} + \text{Kfs} = \text{Sil} + \text{Bt} + \text{Pl}. \quad \text{(R1)}$$

This reaction takes place continuously in the sillimanite + melt field (stippled area on Fig. 6) and has near isothermal isopleths, which indicate a cooling path (Spear et al., 1999; Kohn and Spear, 2000; Vielzeuf and Schmidt, 2001). The anorthite content of plagioclase increases from a uniform composition of ~0.20 in the matrix to ~0.23 in the embayment of resorbed garnet margins, which suggests that decompression accompanied R1 (e.g., Spear, 1993).

Conventional garnet-plagioclase-sillimanite-quartz (GASP) barometry yields an estimate of the pressure peak reached by sample Fg-462a. The uniform plagioclase and grossular composition in this sample justify the assumption of equilibrium necessary for the GASP calculations. However, garnet-biotite thermometry could not be used because it yielded *P-T* conditions below the muscovite-dehydration melting reaction, likely because garnet and biotite composition were modified by Fe-Mg exchange reaction and by R1 (Kohn and Spear, 2000). The temperature input for the GASP calculations were therefore estimated through experimental and numerical phase equilibria modeling of the muscovite-out and biotite-out reactions for metapelitic schists (Vielzeuf and Schmidt, 2001; White et al., 2007). Results (Table 4; Fig. 6) indicate a *P-T* field located immediately

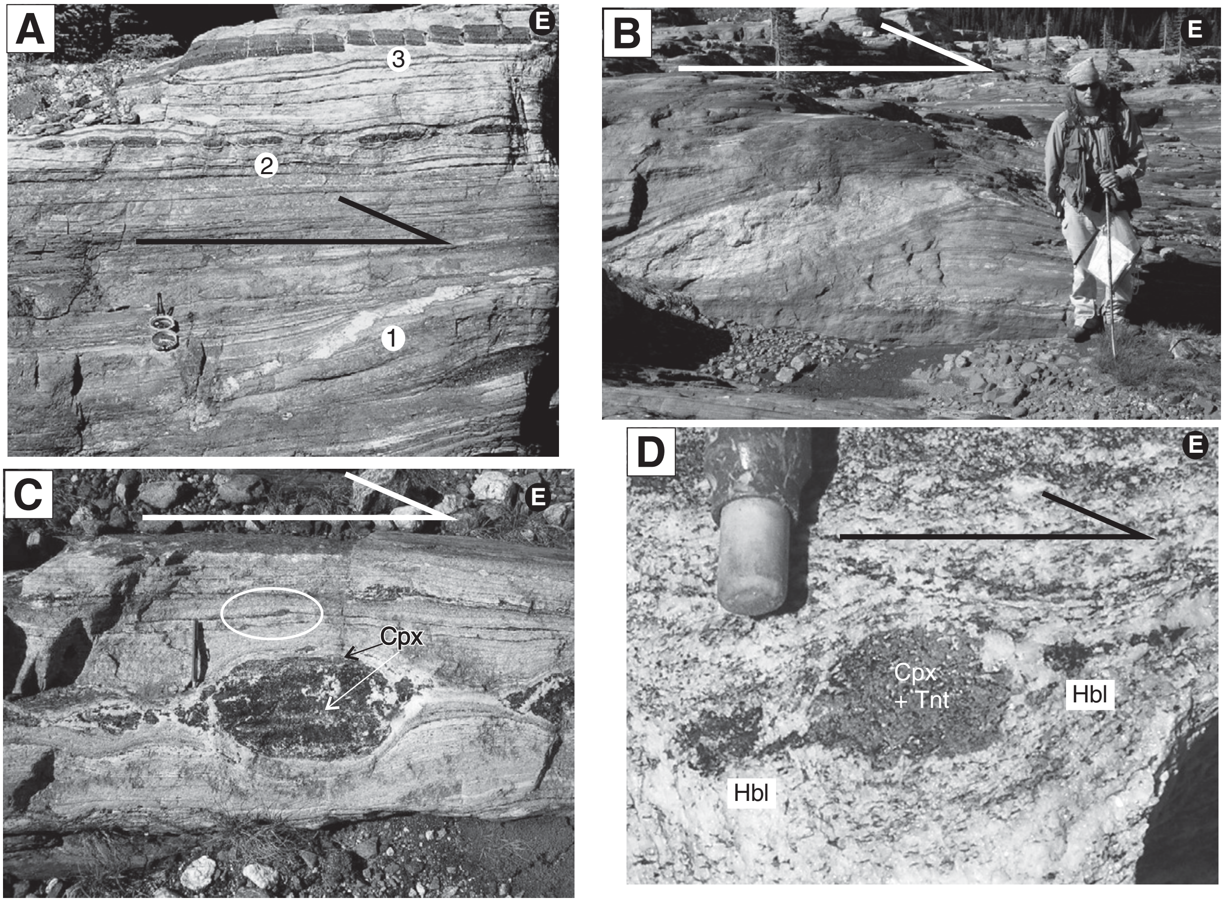

Figure 4. Field photographs from the northern segment of the Monashee décollement (location C on Fig. 1B). All photos show surfaces perpendicular to the foliation and parallel to the stretching lineation. (A) Mylonitic straight gneiss with boudinaged amphibolite layers. Three types of boudins observed on this photograph can be considered as reliable shear sense indicators (Goscombe and Passchier, 2003): (1) foliation-oblique shear-band boudins of a leucogranite dike; (2) foliation-parallel shear-band boudins of an amphibolite layer; and (3) foliation-parallel domino-boudins of an amphibolite layer. Shear sense is invariably top-to-the-E. Compass for scale. (B) Foliation-oblique shear-band boudin in leucogranite indicating a top-to-the-E sense of shear. (C) The center of the photograph is an amphibolite boudin that contains clinopyroxene-bearing (Cpx) leucosome. Leucosome is preferentially located at the neck where amphibolite is broken into angular fragments. These relationships are interpreted as evidence for melt-present deformation. Stair-step structures (Hanmer and Passchier, 1991) in this mylonitic gneiss above the boudin (ellipse) indicate top-to-the-E sense of shear. Pen for scale. (D) Sample FG-462d used for conventional thermobarometry and laser ablation–multicollector–inductively coupled plasma–mass spectrometry U-Pb geochronology of zircon and titanite (Tnt). It consists of a sigma-type clinopyroxene aggregate. Notice preferential location of leucosome in the upper-right and lower-left pressure shadows where hornblende (Hbl) is preferentially crystallized. See text for further explanation. Eraser tip for scale.

below the kyanite-sillimanite reaction between temperatures of 750 °C and 860 °C at pressures of 1200–800 MPa.

Thermobarometry for the Synkinematic Clinopyroxene-Bearing Leucosome Sample Fg-462d

The second sample, Fg-462d, is a leucosome cored by a clinopyroxene-rich aggregate (Fig. 4D). The aggregate is an intergrowth of coarse-grained and euhedral to subhedral grains of clinopyroxene, titanite, plagioclase, K-feldspar, and quartz, whereas the host rock consists of aligned, medium-grained and recrystallized feldspar, quartz, biotite, and hornblende grains (Fig. 5B). The intergrowth texture (Fig. 5C), the euhedral shape of grains (Fig. 5C), and the sharp adjacent crystal faces (Fig. 5D) are interpreted as evidence for growth of clinopyroxene and titanite in the presence of melt, whereas the microstructures in the host gneiss indicate solid-state deformation (cf. Vernon, 2004). The concentration of leucosome into the asymmetric pressure shadows of the aggregate (Fig. 4D) further suggests migration of the melt phase during top-to-the-E shearing, which promoted the pseudomorphism of clinopyroxene by hornblende (Fig. 5D).

Conventional thermobarometry was conducted on sample Fg-462d. Clinopyroxene, hornblende, and plagioclase are unzoned, and their compositions do not vary with textural setting (Table 3). Table 4 and Figure 6 show the results of thermobarometry for sample Fg-462d using the average-pressure method of Thermocalc version 3.1 (Powell and Holland, 1994), the SCAn barometer (McCarthy and Patiño-Douce, 1998), and the hornblende-plagioclase thermometer (Holland and Blundy, 1994). The uniform compositions of clinopyroxene, plagioclase, and hornblende in specimen Fg-462d, combined with the excellent σ_{fit} = 1.0–1.1 for three independent reactions obtained by Thermocalc (see Powell and Holland, 1994), indicate that equilibrium between these three minerals was reached. Inasmuch as hornblende is interpreted to have formed during crystallization

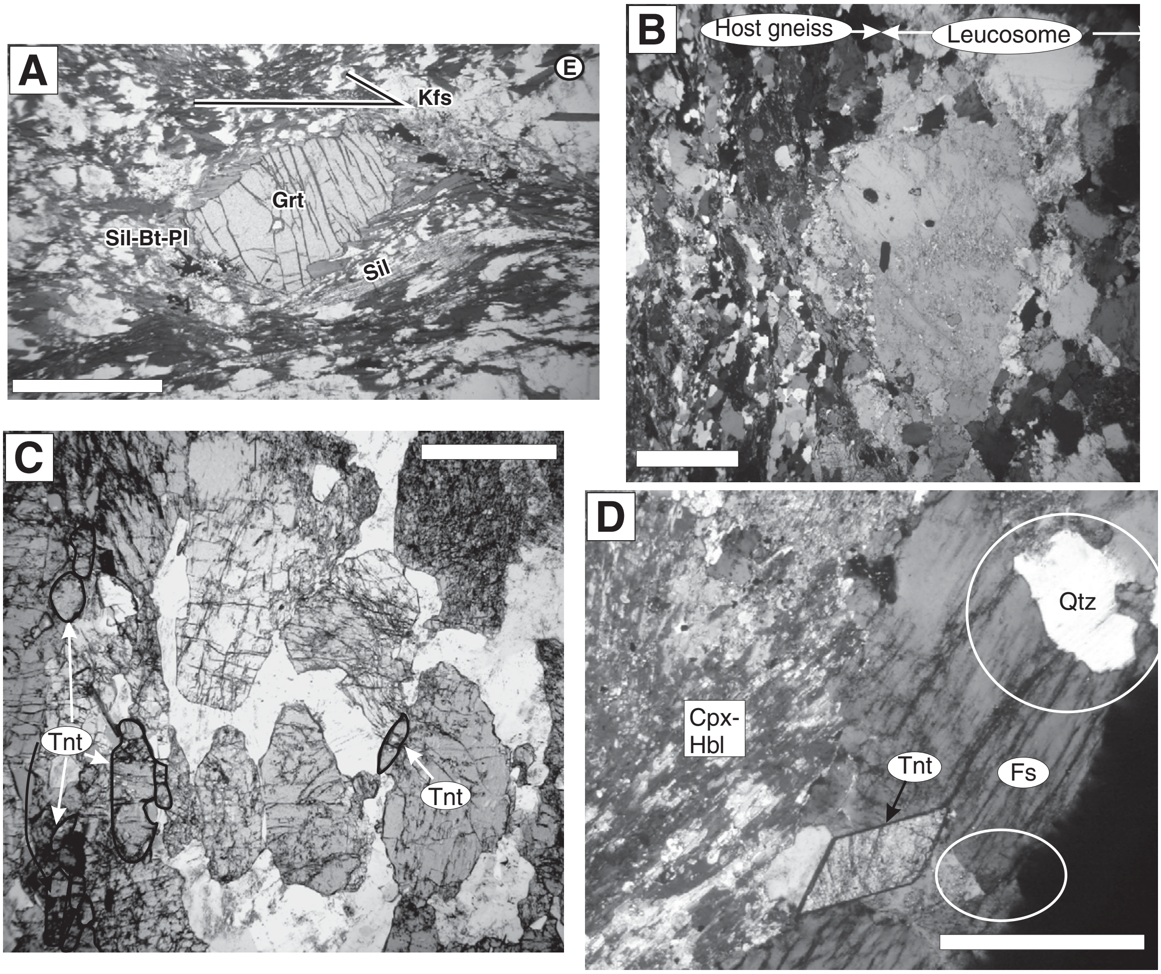

Figure 5. Photomicrographs for samples Fg-462a and Fg-462d. (A) One of the rare garnets in sample Fg-462a, a migmatitic pelitic schist. The long axis of this oblate garnet is inclined relative to the foliation (which is parallel to the length of the picture) and is oriented from bottom-left to top-right of the image. Notice that sillimanite-biotite-plagioclase (Sil-Bt-Pl) are concentrated in garnet pressure shadows, which is evidence for dynamic garnet resorption by R1 during top-to-the-E shearing (dextral on the picture). Thin section is cut parallel to the lineation and perpendicular to the foliation. (B) Contact between host and leucosome of sample Fg-462d. Note the coarse grain size and euhedral shape of quartz (Qtz) and feldspar (Fs) grains forming the leucosome. (C) Core of the clinopyroxene (Cpx) aggregate of sample Fg-462d. Note the euhedral and faceted shape of clinopyroxene and titanite (Tnt), as well as the intergrowth texture between these two minerals. (D) Margin of the clinopyroxene aggregate of sample Fg-462d where clinopyroxene is directly pseudomorphed into hornblende (Hbl). Note the perfect crystalline shape of titanite and crystal faces of feldspar and quartz crystals. Observations in B–D are interpreted as evidence for the growth of clinopyroxene and titanite in the presence of a melt phase. Scale bar is 1 mm long on all photomicrographs.

of a melt phase, the quartz-saturated hornblende-plagioclase thermometer (Fig. 6; Holland and Blundy, 1994) is preferred because it yields a temperature closer to the wet-granite solidus (Fig. 6). The average pressure of ~270 MPa at 700 °C calculated with Thermocalc (Fig. 6) is consistent with the pressure of ~285 MPa and 700 °C calculated by the SCAn barometer (Fig. 6). The preferred *P-T* conditions of equilibrium during hornblende formation in sample Fg-462d are thus estimated at ~700 °C and 300 MPa (Fig. 6).

U-Pb Geochronology

Zircon Results. Twenty-six U-Pb analyses were obtained from 18 zircon grains extracted from sample Fg-462d (for analytical methods, see Appendices). Zircon commonly consists of rounded cores surrounded by euhedral and elongated rims with sharp crystal faces (Figs. 7A–7C). Cathodoluminescence (CL) images reveal a sector to faint oscillatory zoning (Figs. 7A–7C; Corfu et al., 2003). Grain L02 (CL image in Fig. 7A) is interesting because it exhibits an euhedral core overgrown by an euhedral rim separated by a dark thin band spatially associated with minor resorption textures. U-Pb dates of rounded cores range in age from Archean to Devonian (Table 5) and are interpreted to reflect xenocrystic inheritance. U-Pb dates of zircon rims that fall on, or near, concordia yield dates of ca. 120, 107, 83, and 62 Ma, with two clusters at ca. 83 Ma and ca. 62 Ma. The older cluster of rim dates, which represents four analyses from three grains including grain L02, yields a weighted mean average $^{206}Pb/^{238}U$ age of 82 ± 4 Ma (mean square of weighted deviates [MSWD] = 1.6; probability of fit (prob.) = 0.19; Fig. 7D). The younger cluster of rim dates, which represents five analyses from four grains including grain L02, yields a

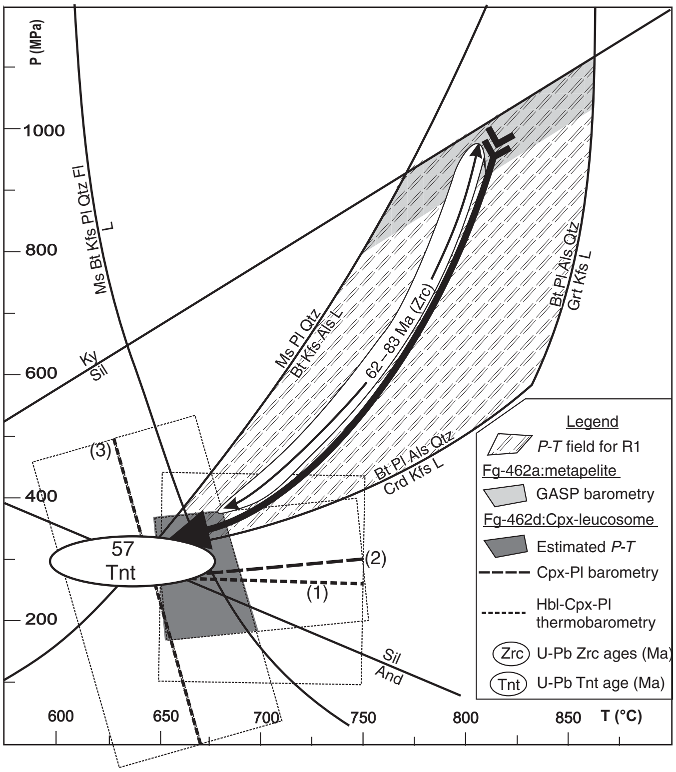

Figure 6. Pressure-temperature-time (*P-T-t*) path for the northern segment of the Monashee décollement (station C on Fig. 1B). Background shows lines of disappearance/appearance of key metamorphic assemblages for typical pelitic schists deduced from experimental (Vielzeuf and Schmidt, 2001) and thermodynamic modeling (White et al., 2007). R1 takes place continuously along any cooling path within the stippled area. Also shown are *P-T* conditions estimated with conventional thermobarometry analyses conducted on samples Fg-462a and Fg-462d. Curve 1 is the result of the average *P* mode in Thermocalc. Curve 2 is the SCAn barometer of McCarthy and Patiño-Douce (1998). Curve 3 is the quartz-saturated hornblende-plagioclase thermometer of Holland and Blundy (1994). Stippled boxes are the uncertainties associated with thermobarometry. Explanation of the *P-T-t* path is given in the text. Mineral abbreviations are after Kretz (1983). GASP—Garnet-plagioclase-sillimanite-quartz barometer. Abbreviations: Ms—muscovite; Bt—biotite; Kfs—K-feldspar; Pl—plagioclase; Qtz—quartz; Fl—fluid; Ky—kyanite; Sil—sillimanite; Als—aluminosilicates; Grt—garnet; Crd—cordierite; L—liquid; Cpx—clinopyroxene; Hbl—hornblende; Zrc—zircon; Tnt—titanite; And—andalusite.

TABLE 3. CHEMICAL COMPOSITION OF MINERALS USED FOR THERMOBAROMETRY

	Fg-462d			Fg-462a	
Mineral	Cpx	Hbl	Pl	Grt 1	Pl
	Average (6)	Average (5)	Average (6)	Core (2)	Average (5)
SiO_2	53.03	48.66	65.89	37.41	64.18
TiO_2	0.12	0.47	0.00	0.01	0.00
Al_2O_3	1.51	5.48	21.67	21.16	23.51
Fe_2O_3	2.51	2.15	0.19	0.52	0.00
FeO	8.05	12.60	0.00	31.21	0.00
MnO	0.59	0.44	0.00	2.74	0.22
MgO	11.38	13.07	0.00	5.35	0.00
CaO	21.65	10.96	2.31	1.47	4.31
Na_2O	1.47	1.31	10.28		9.21
K_2O	0.01	0.64	0.26		0.21
Total	100.07	95.56	100.60	99.86	101.64
Oxygens	6.00	23.00	8.00	12.00	8.00
Si	1.98	7.27	2.88	2.98	0.00
Ti	0.00	0.05	0.00	0.00	2.03
Al	0.07	0.97	1.12	1.99	0.49
Fe^3	0.07	0.24	0.01	0.00	0.37
Fe^2	0.25	1.57	0.00	2.11	0.00
Mn	0.02	0.06	0.00	0.18	0.01
Mg	0.63	2.91	0.00	0.64	0.00
Ca	0.87	1.75	0.11	0.13	0.20
Na	0.11	0.38	0.87		0.78
K	0.00	0.12	0.02		0.01
Sum	4.00	15.41	5.00	8.00	5.00
Na/Na+Ca	0.11		0.89		0.79
Fe/Fe+Mg	0.34	0.35		0.77	
Xpyr				0.21	
Xgrs				0.04	
Xsps				0.06	

Note: Number in parentheses refers to the number of analyses used in the average calculation. Abbreviations: cpx—clinopyroxene; Hbl—hornblende; Pl—plagioclase; Grt—garnet.

TABLE 4. RESULTS OF THERMOBAROMETRY FOR SAMPLES FG-462d AND FG-462a

Thermobarometer	*P* (MPa)	±1σ	*T* (°C)	±1σ
Fg-462d				
Average *P* Thermocalc v. 3.1*	280–260#	130	650–750	n.a.
SCAn†	270–300#	100	650–750	n.a.
Hbl-Pl§	0–500	n.a.	670–630**	40
Fg-462a				
GASP††	800–1200	80	750–860§§	50

*Based on three independent equilibria; with the SCAn reactions discarded, it yields a σ_{fit} = 1.0 (Powell and Holland, 1994).
†Ca-tschermak (cpx) + qtz = An (McCarthy and Patiño-Douce, 1998).
§Qtz saturated (Holland and Blundy, 1994).
#*P* calculated at specific temperatures listed under the "*T*" column.
***T* calculated at specific pressures listed under the "*P*" column.
††Garnet-plagioclase-sillimanite-quartz barometer of Holdaway (2001).
§§Temperature range between the muscovite-out and biotite-out reactions estimated from experimental (Vielzeuf and Schmidt, 2001) and thermodynamic modeling (White et al., 2007) studies.
Abbreviations: Hbl—hornblende; Pl—plagioclase; cpx—clinopyroxene; qtz—quartz.

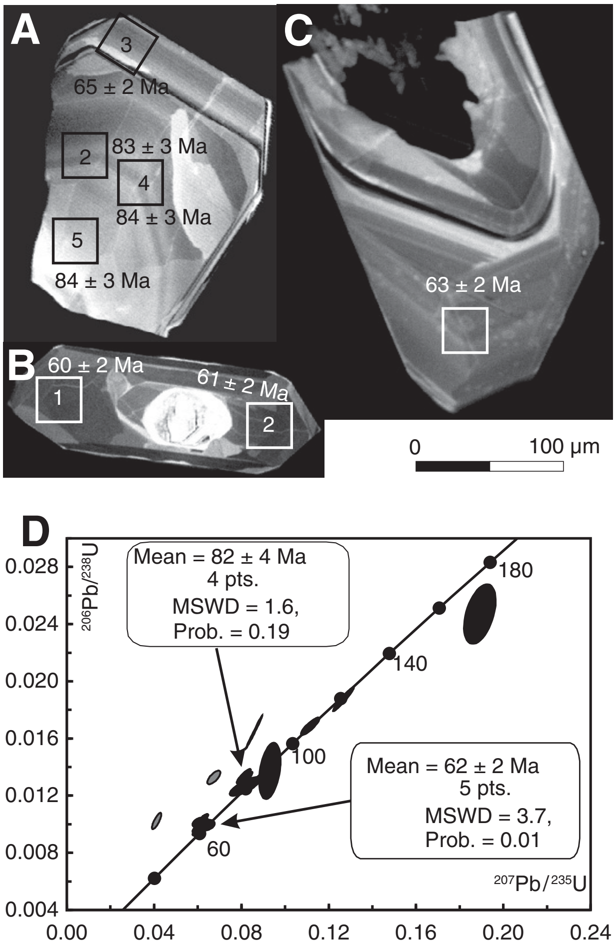

Figure 7. Laser ablation–multicollector–inductively coupled plasma–mass spectrometry zircon U-Pb geochronology of clinopyroxene-bearing leucosome sample Fg-462d. (A–C) Cathodoluminescence images of zircon with location of analysis spot with $^{206}Pb/^{238}U$ date (error is 2σ). Notice the sharp crystal faces and the zoning in A and C. (D) Concordia plot showing the distribution of metamorphic dates. The two analyses lying above the concordia curve (gray ellipses) were discarded for the calculations of the weighted mean $^{206}Pb/^{238}U$ ages of the two clusters. Part D was plotted with Isoplot 3 (Ludwig, 2008). MSWD—mean square of weighted deviates; Prob.—probability of fit.

TABLE 5. U-Pb LASER ABLATION–MULTICOLLECTOR–INDUCTIVELY COUPLED PLASMA–MASS SPECTROMETRY SPOT ANALYSES OF ZIRCON GRAINS FROM LEUCOSOME SAMPLE 05-FG-462d

Analysis no.	$^{207}Pb/^{235}U$	±2σ	$^{206}Pb/^{238}U$	±2σ	ρ	$^{206}Pb/^{238}U$ age (Ma)	±2σ (Ma)
Rims							
S02-2*	0.1889	0.0060	0.0247	0.0017	0.45	157	11
S03-1	0.1112	0.0035	0.0167	0.0005	0.86	107	3
S05-2	0.1262	0.0040	0.0187	0.0007	0.96	119	4
L02-2	0.0814	0.0027	0.0130	0.0004	0.90	83	3
L02-3	0.0615	0.0022	0.0101	0.0003	0.85	65	2
L02-4	0.0806	0.0027	0.0132	0.0004	0.87	84	3
L02-5*	0.0668	0.0024	0.0131	0.0004	0.71	84	3
S05-1*	0.0853	0.0030	0.0164	0.0010	0.99	105	6
S12	0.0927	0.0041	0.0136	0.0016	0.36	87	10
S13	0.0599	0.0023	0.0093	0.0003	0.76	60	2
S13-2	0.0603	0.0025	0.0095	0.0003	0.64	61	2
S15	0.0634	0.0032	0.0097	0.0003	0.30	62	2
S15-2*	0.0405	0.0018	0.0100	0.0005	0.79	64	3
S16	0.0608	0.0029	0.0099	0.0003	0.36	63	2
S19-1	0.0813	0.0058	0.0125	0.0005	0.78	80	4
Detrital							
02-1	4.5261	0.1359	0.2858	0.0107	0.96	1620	61
04-1	11.6970	0.3510	0.4400	0.0146	0.94	2351	78
08-1	0.5103	0.0154	0.0650	0.0021	0.92	406	13
09-1	0.6671	0.0201	0.0822	0.0027	0.94	509	17
11-1	0.8458	0.0254	0.0987	0.0033	0.95	607	20
L01-1	2.0724	0.0622	0.1920	0.0064	0.94	1132	38
L01-2	2.0084	0.0603	0.1893	0.0064	0.93	1118	38
S03-1	0.5549	0.0175	0.0718	0.0057	0.40	447	36
S07-1	0.6482	0.0198	0.0845	0.0045	0.58	523	28
S23-1	0.7095	0.0216	0.0805	0.0043	0.56	499	27

Note: Spot size is 40 × 40 µm except for analyses labeled with asterisk, for which the spot size was 20 × 20 µm.

weighted mean average $^{206}Pb/^{238}U$ age of 62 ± 2 Ma (MSWD = 3.7; prob. fit = 0.01; Fig. 7D). The morphology of zircon grains and the overgrowth relationship of grain L02, which is formed by a ca. 82 Ma core and a ca. 62 Ma rim, suggest the presence of a melt phase (Corfu et al., 2003) during the two main periods of zircon growth.

Titanite Results. Titanite in sample Fg-462d is ~300 × 600 µm, euhedral, and in textural equilibrium with clinopyroxene and plagioclase (Figs. 5C and 5D). Titanite has dark cores surrounded by light rims when examined on backscattered electron images (Figs. 8A–8D). Regression of 21 of the 22 uncorrected analyses on a Tera-Wasserburg plot intersects concordia at 58 ± 9 Ma (MSWD = 18) and yields a *y*-axis $^{207}Pb/^{206}Pb$ intercept of 0.65 ± 0.13 (Fig. 8E). Using the *y*-axis for common Pb correction (Storey et al., 2006; Aleinikoff et al., 2007), we find a corrected weighted mean average $^{206}Pb/^{238}U$ age of 57 ± 2 Ma (MSWD = 1.00; prob. = 0.46; Fig. 8F; Table 6). There is no difference in age between cores and rims, even if treated separately for common Pb correction. We interpret this ca. 57 Ma age as the time at which the sample cooled below the closure temperature for Pb diffusion in titanite (600–680 °C, depending on the cooling rate for grains of this size; Cherniak, 1993).

P-T-t Path for the Monashee Décollement. The data presented here allow the construction of the retrograde *P-T-t* path followed by rocks of the northern segment of the Monashee décollement. The record of zircon growth in leucosome sample Fg-462d (Fig. 7D) indicates protracted high-temperature metamorphism between 120 and 62 Ma, typical of lower Selkirk allochthon rocks (Table 2). Peak metamorphic conditions were reached some time in this period and are estimated at 800–1200 MPa and 750–860 °C from the migmatitic pelitic schist sample Fg-462a (Fig. 6). Thermobarometric results indicate that the synkinematic clinopyroxene-bearing leucosome sample Fg-462d equilibrated at *P-T* conditions of ~300 MPa and 700 °C (Fig. 6; Table 4). The retrograde *P-T* path, therefore, involved >500 MPa of decompression at high temperature. Top-to-the-E shearing was taking place during decompression because the shear fabric is formed by the product of the retrograde reaction R1. A key to deriving the timing of this path is the presence of a melt phase in sample Fg-462d. Indeed, evidence presented here indicates the presence of melt during: (1) the growth of zircon at ca. 82 and ca. 62 Ma (Fig. 7D); (2) the growth of the synkinematic clinopyroxene-titanite aggregate (Figs. 4D, 5C, and 5D); and (3) the retrogression of clinopyroxene to hornblende in the top-to-the-E asymmetric pressure shadow of the aggregate that equilibrated at ~300 MPa and ~700 °C (Figs. 4D and 5D). However, melt was most likely crystallized at ca. 57 Ma when Pb ceased to diffuse in titanite. Hence, the

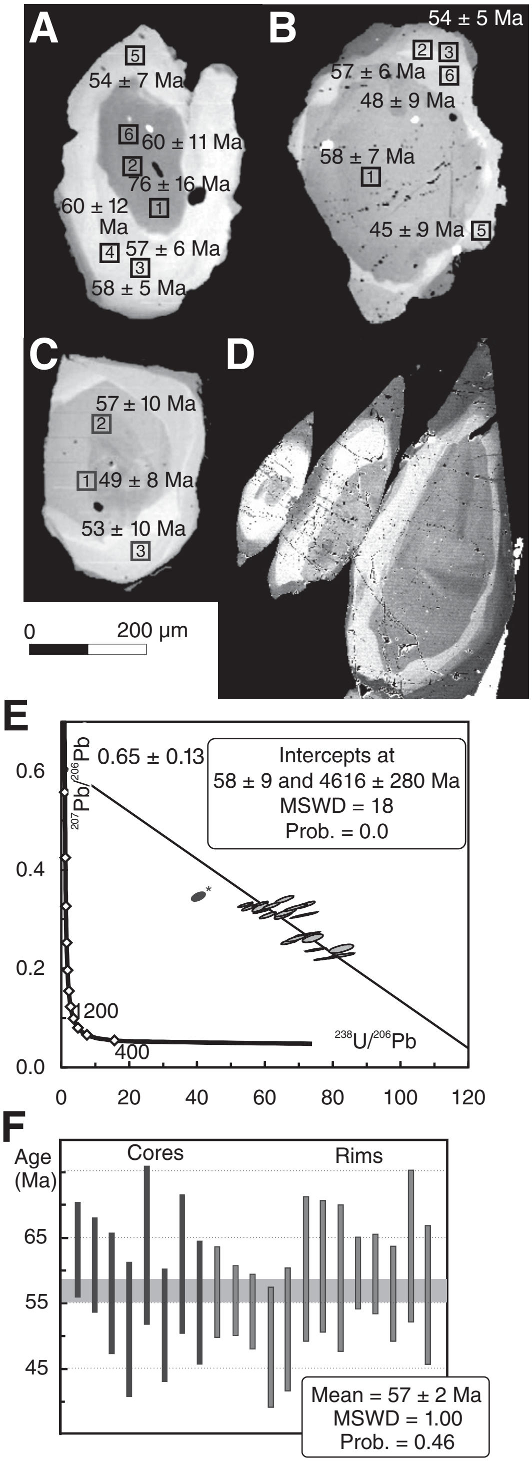

Figure 8. Laser ablation–multicollector–inductively coupled plasma–mass spectrometry titanite U-Pb geochronology of clinopyroxene-bearing leucosome sample Fg-462d. (A–D) Backscattered electron (BSE) images of titanite and location of analysis spot with $^{206}Pb/^{238}U$ date (error is 2σ). Note the euhedral shape of the grains on the microphotograph in D. (E) Tera-Wasserburg plot. Upper intercept on the *y*-axis is interpreted as the initial common Pb composition and lower intercept as the age of the titanite. (F) Weighted mean $^{206}Pb/^{238}U$ age of 57 ± 2 Ma age is interpreted as the time at which these titanite grains closed to Pb diffusion. E and F were plotted with Isoplot 3 (Ludwig, 2008). MSWD—mean square of weighted deviates; Prob.—probability of fit.

TABLE 6. U-Pb LASER ABLATION–MULTICOLLECTOR–INDUCTIVELY COUPLED PLASMA–MASS SPECTROMETRY SPOT ANALYSES OF TITANITE GRAINS FROM LEUCOSOME SAMPLE 05-FG-462d

	Uncorrected isotopic ratios and errors				Corrected age†	
	$^{238}U/^{206}Pb$	±2σ	$^{207}Pb/^{206}Pb$	±2σ	Age (Ma)	±2σ
Cores						
M01-1	67.227	2.173	0.25219	0.00522	63	7
M02-1	68.889	2.200	0.25796	0.00517	61	7
M04-1	65.200	2.174	0.30602	0.00630	56	9
M05-1	65.463	2.231	0.33842	0.00646	51	10
S01-1	53.912	1.739	0.32762	0.00451	64	12
S01-2*	40.464	1.241	0.33946	0.00416	82	17
S05-1	71.320	3.153	0.30644	0.00510	51	9
S05-2	58.735	2.008	0.31510	0.00402	61	11
S12	65.826	2.615	0.31145	0.00654	55	10
Rims						
M01-2	73.874	2.532	0.25850	0.00730	56	7
M02-2	82.452	3.053	0.22303	0.00424	55	5
M02-3	82.378	2.952	0.23682	0.00717	53	6
M02-5	71.702	2.370	0.32755	0.00563	48	9
M02-6	68.875	2.814	0.32216	0.00576	51	9
M03-1	58.193	1.858	0.32234	0.00703	60	11
M04-2	60.583	2.077	0.30621	0.00532	60	10
M05-2	58.319	1.981	0.32900	0.00457	59	11
S01-3	77.718	2.892	0.21653	0.00276	59	5
S01-4	74.764	2.557	0.23432	0.00316	59	6
S01-5	72.543	2.814	0.26730	0.00303	56	7
S01-6	55.065	1.842	0.32163	0.00509	63	12
S05-3	61.637	2.015	0.32573	0.00556	56	11

*Discarded from calculations.
†$^{206}Pb/^{238}U$ age corrected for common Pb (see text for details).

estimated *P-T* of equilibration (Fig. 6) is tightly bracketed between 62 and 57 Ma (Fig. 6). This is consistent with the ca. 57 Ma age of the leucogranite suite crosscutting the foliation at this outcrop (Scammell, 1993). Consequently, the northern segment of the Monashee décollement was shearing along a high-temperature decompression path before ca. 62 Ma and the last increments of top-to-the-E shearing occurred between 62 and 57 Ma at *P-T* conditions of ~300 MPa and 700 °C.

P-T-t Path for the Lower Selkirk Allochthon NE of the Monashee Complex

Scammell (1993) constructed a *P-T-t* path for lower Selkirk allochthon rocks between locations A and B (Fig. 1B). Scammell was the first to point out that a large amount of top-to-the-E shear strain accumulated along a cooling path by R1 because the foliation, lineation, and many kinematic indicators are formed by its products. From a detailed analysis taking into account the effect of Fe-Mg exchange reactions between biotite and garnet, as well as the effect of R1, Scammell (1993) estimated peak metamorphic conditions at 700–800 °C and 700–900 MPa and retrograde conditions at ~450 MPa and 600 °C. This 300–500 MPa of decompression at high temperature is consistent with our results for location C. The timing of this synshearing exhumation episode was bracketed between ca. 100 Ma, the U-Pb ages of transposed leucogranites and U-Pb monazite ages in schist, and ca. 90 Ma, the oldest U-Pb titanite age at location A (Fig. 1B). Scammell used this latter age rather than the ca. 74 Ma titanite age obtained at location B because he assumed that cooling was synchronous throughout the entire area. However, based on the trend of cooling ages reported in Figure 3B here, we reinterpret these two different ages as indicative of this trend. Inasmuch as similar retrograde *P-T* paths and timing of high-temperature metamorphism were recorded at locations A, B, and C, the trend of cooling ages implies successive high-temperature decompression paths becoming younger southwestward, as shown in Figure 9.

P-T-t Path for the Monashee Complex

Foster et al. (2004) derived a prograde *P-T-t* path for a migmatitic kyanite-bearing schist collected by Gibson et al. (1999) in the footwall of the Monashee décollement near location D in the northern Frenchman Cap dome (Fig. 1B). The path involves heating and burial in the kyanite field between ca. 75 and 56 Ma and a peak pressure estimate of ~1000 MPa. These results are consistent with the ca. 58 Ma estimate for the timing at which migmatitic schists from a similar structural level, but on the west flank of the dome, reached the kyanite + melt field (Crowley and Parrish, 1999; Crowley et al., 2001). The end of ductile deformation is constrained at ca. 55 Ma from the age of a crosscutting pegmatite and from a hornblende $^{40}Ar/^{39}Ar$ plateau age (Crowley and Parrish, 1999). Because kyanite in the ca. 58 Ma leucosomes is pseudomorphed by andalusite and because synkinematic andalusite has been observed nearby (Journeay, 1986; Scammell, 1986), there must have been significant decompression between ca. 58 and 55 Ma (Fig. 3C). Although slightly older, these results are consistent with the near-isothermal, high-temperature decompression path between 56 and 51 Ma documented in the Thor-Odin dome (Norlander et al., 2002; Hinchey et al., 2006).

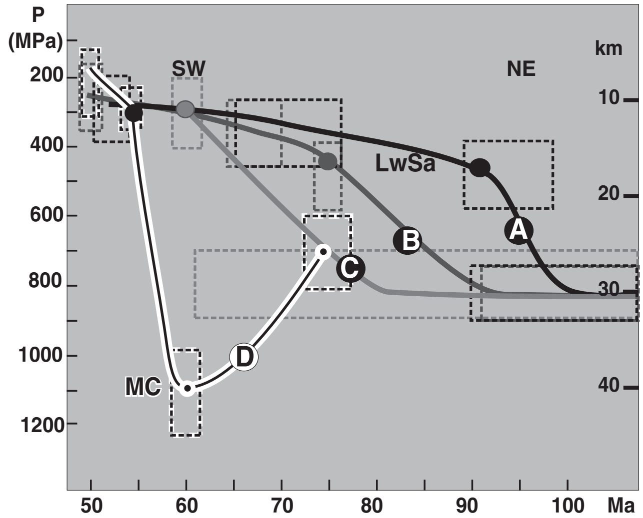

Figure 9. Depth-time paths for the lower Selkirk allochthon and underlying Monashee Complex (MC). Notice the age of exhumation becomes younger from A to C along a SW azimuth, and that the exhumation of the lower Selkirk allochthon (LwSa; A–C) was coeval with burial of the MC (D). Filled circles are well-constrained pressure-temperature-time (*P-T-t*) points. Stippled rectangles are uncertainties on pressures and timing. Sources of data are presented in Table 2. See text for explanation.

Timing of Motion of the Two Oppositely Verging Shear Zones Bounding the Lower Selkirk Allochthon

A key criterion for testing tectonic models of exhumation is the timing of shearing along reverse and normal shear zones (Fig. 2). The existence of the Monashee décollement has been questioned by Vanderhaeghe et al. (1999), Williams and Jiang (2005), and Kruse and Williams (2007). However, the contrast in plutonic history (Table 2) and the contrast in depth-time paths (Fig. 9) between the lower Selkirk allochthon and the Monashee Complex clearly demonstrate that the two units were not juxtaposed until the Eocene. Furthermore, results presented herein for the northern segment agree with those obtained previously for the southern segment (Carr, 1992, 1995) and confirm that the last increments of top-to-the-E shearing along the reverse shear zone took place between 62 and 57 Ma along its entire length. The contrast in lithologic units may be less striking in the south than in the north (but see McNicoll and Brown, 1995), but the similarities in structure, metamorphism, and timing of shearing demonstrate that the Monashee décollement bounds the west flank of the Monashee Complex along its entire length. It is not possible to determine if shearing started earlier than ca. 62 Ma, but the protracted high-temperature conditions recorded by zircon growth in leucosomes and sheared leucogranites of this shear zone (continuous record from 100 to 58 Ma; Table 2) suggest that it did.

A general *P-T-t* trend for the Okanagan Valley fault system can be estimated from the metamorphic paragenesis in top-to-the-W microstructures combined with the timing of synkinematic intrusions and cooling ages. Top-to-the-W kinematic indicators are formed by: (1) the peak metamorphic minerals biotite–sillimanite-garnet-K-feldspar; (2) biotite-sillimanite folia in pressure shadows of resorbed garnet (Bardoux, 1993; Glombick et al., 2006a; Johnson, 2006); (3) retrograde minerals muscovite and chlorite; and (4) brittle structures (Bardoux, 1993; Johnson, 2006). This sequence indicates that shearing started at the thermal peak, continued along a cooling path, first at high temperature during garnet breakdown by R1, and then at lower temperature during crystallization of hydrous minerals, and finally ended in the brittle field. As for the Monashee décollement, the record of zircon growth in leucosomes from 100 to 57 Ma indicates protracted high-temperature conditions. Furthermore, the overlap between the intrusion of the synkinematic Ladybird leucogranite and hornblende Ar/Ar cooling ages implies that the last increments of top-to-the-W ductile shearing along the Okanagan Valley fault system took place between 60 and 56 Ma (Table 2; Carr, 1992; Johnson, 1994; Vanderhaeghe et al., 1999). It is not possible to ascertain if shearing started earlier, but the protracted record of zircon growth in sheared leucosome between 100 and 57 Ma suggests that it did.

The two shear zones bounding the lower Selkirk allochthon therefore share the same structural, metamorphic, and geochronological characteristics (Table 7). Combined with the high-temperature decompression path documented previously (Fig. 6), these similarities imply that the lower Selkirk allochthon was approaching the surface of Earth by coeval shearing along the top-to-the-E Monashee décollement at its base and the top-to-the-W Okanagan Valley fault system at its roof in the Paleocene.

TABLE 7. COMPARISON MONASHEE DÉCOLLEMENT (MD) VS. OKANAGAN VALLEY FAULT SYSTEM (OVFs)

	MD	OVFs
Shear sense	Top-to-the-E	Top-to-the-W
Metamorphic grade	Sil-Kfs	Sil-Kfs
P-T path	↓T, ↓P	↓T, ↓P?
Timing HT	118–59 Ma	120–57 Ma
Timing last increments HT shear strain	62–57 Ma*	60–56 Ma
Timing end of ductile deformation	ca. 57 Ma	Down to ca. 49 Ma
Timing cooling <500–600 °C	59–57 Ma	58–54 Ma

Note: HT—high temperature.
*New data.

TESTING THE EXHUMATION MODELS

In this section, the newly devised test of exhumation processes in collisional orogens (Fig. 2D) is applied to the area surrounding the Monashee Complex in the southeastern Canadian Cordillera. The three main modes of exhumation are ranked from least to most plausible based on a comparison of the data set described herein with the predictions of analogue and numerical models of collisional orogens (Fig. 2D).

Gravitational Collapse

Most studies have attributed the exhumation of midcrustal rocks in the southeastern Canadian Cordillera to the gravitational collapse of a thickened welt following a reduction of convergence rate and/or delamination of the mantle lithosphere in the Eocene (Coney and Harms, 1984; Tempelman-Kluit and Parkinson, 1986; Parrish et al., 1988; Carr, 1992; Bardoux and Mareschal, 1994; Vanderhaeghe and Teyssier, 1997; Liu, 2001; Norlander et al., 2002; Teyssier and Whitney, 2002; Price and Monger, 2003; Teyssier et al., 2005; Kruse and Williams, 2007; Rey et al., 2009). Our test could be partially compatible with the gravitational collapse model (Fig. 2D) if applied to the area south of the Frenchman Cap dome, where most of the aforementioned studies were conducted, but it would not be compatible if applied to the area surrounding the dome (e.g., cross section of Fig. 3A). However, the continuity of the lower Selkirk allochthon from west of the Thor-Odin dome to the northern Monashee Mountains (Fig. 1), which is well marked by similar lithological, structural, metamorphic, and geochronological characteristics, requires the incorporation of the entire area into the test. Hence, the absence of a major normal shear zone in the northern Monashee Mountains (Figs. 1 and 3A), the prevalence of finite strain indicative of general shear rather than horizontal flattening, and moreover the synchronous exhumation of the lower Selkirk allochthon and burial of the Monashee Complex (Fig. 9) rule out gravitational collapse as the preferred exhumation mode of the lower Selkirk allochthon. As for the Monashee Complex, the absence of a penetrative fabric of Cordilleran age, the preservation of Paleoproterozoic Pb in titanite, as well as the 52–49 Ma contractional structures in felsic gneisses located 5 to 10 km structurally below the kyanite–K-feldspar migmatites of the upper part of the complex imply late basement underthrusting (cf. Gervais et al., 2010). This, in turn, implies that the exhumation of these kyanite-migmatites to the andalusite field between 59 and 55 Ma occurred during convergence. A synconvergent mode of exhumation is therefore required for both the lower Selkirk allochthon and the upper part of the Monashee Complex.

Orogenic Wedge

The orogenic wedge mode was proposed mainly based on data collected in and north of the Frenchman Cap dome (Brown and Journeay, 1987; Parrish, 1995; Brown, 2004) and has not been tested against predictions from modeling studies (Fig. 2A). The first prediction common to all models is that of reverse shearing localized at the retro-shear zone and steep flattening in the wedge interior. In contrast, a shallowly dipping transposition foliation formed by reverse shear strain is distributed through the 16–20-km-thick package of high-grade rocks consisting of the lower Selkirk allochthon and Monashee Complex. The sharp transition from migmatites to greenschist-facies rocks across the Okanagan Valley fault system, as well as the absence of a cooling age gradient in the lower Selkirk allochthon west of the Monashee Complex are both not compatible with this exhumation mode. Furthermore, the coeval motion of major normal (Okanagan Valley fault system) and reverse (Monashee décollement) shear zones bounding the lower Selkirk allochthon is difficult to reconcile with an orogenic wedge model. The model of vertical normal shearing at the top of an uplifting duplex stack (Fig. 2A; Malavieille, 2010) is not applicable either, because this model requires a systematic gradient in peak metamorphic and cooling ages across structural levels. Finally, theoretical considerations suggest that wedge geometry could not have been maintained for a low-viscosity middle crust inferred from the large volume of migmatitic rocks in the lower Selkirk allochthon (Vanderhaeghe et al., 2003a). Therefore, another synconvergent model is required.

Channel Flow and Ductile Extrusion

The first model proposing that part of the exhumation of the lower Selkirk allochthon occurred during convergence and involved crustal decoupling and ductile flow was the "dynamic spreading" model of Scammell (1993). A ductile extrusion model was later proposed by Johnston et al. (2000), and arguments in favor (Brown and Gibson, 2006; Glombick et al., 2006a; Kuiper et al., 2006) and against (Carr and Simony, 2006) the channel-flow concept have recently been put forward. The coeval, but opposite motion of two shear zones bounding the migmatitic lower Selkirk allochthon (Fig. 3A; Table 7), the lateral trend of cooling ages (Figs. 3B and 9), the protracted residence time at high temperature of the lower Selkirk allochthon, and the synchronous exhumation of the lower Selkirk allochthon and burial of the Monashee Complex in its footwall (Figs. 3C and 9) are predicted features common to all channel-flow models (Fig. 2B; Table 2). The sharp transition from migmatitic to greenschist-facies rocks in the hanging wall of the Okanagan Valley fault system and the absence of a sharp metamorphic field gradient in the footwall of the Monashee décollement are not. However, Jamieson et al. (2004) acknowledged that the incorporation of strain localization in the numerical code could lead to a sharper gradient in the hanging wall of a hot channel, which could be an explanation for the observations. The absence of a gradient in the footwall of the lower Selkirk allochthon is explained by the downward migration of flow, as explained in the following. In contrast to the other models, most of the requirements of this exhumation mode are thus met (Fig. 2B), and we argue that a channel-flow process similar to the HT111 model of Jamieson et al. (2006; Fig. 2B) led to the exhumation the lower Selkirk allochthon in the Late Cretaceous to Paleocene.

The extensive multidisciplinary data set compiled herein allows us to derive an internally consistent tectonic model (Fig. 10). Building on the model of Gibson et al. (2008), we propose that rocks of the Selkirk allochthon (both the upper Selkirk allochthon and lower Selkirk allochthon) were deformed and metamorphosed in a SW-verging prowedge in the Jurassic. Whereas rocks of the upper Selkirk allochthon were exhumed to upper-crustal levels (<10–15 km depth) in Jurassic to Early Cretaceous time, rocks of the lower Selkirk allochthon remained at depth and were transported in a retrowedge setting where they continued to be thickened and heated. This reconciles the record of Jurassic metamorphic ages in both the upper and lower panels, whereas Jurassic cooling ages are recorded only in the upper Selkirk allochthon (Table 2; Gibson et al., 2008). The thermal peak was reached at ca. 100–90 Ma, when a significant portion of the middle crust reached partial melting conditions, as recorded by numerous zircon and monazite U-Pb ages in sheared leucosome, leucogranite, and schists of the lower Selkirk allochthon. Building on the models of Scammell (1993), Brown and Gibson (2006), and Glombick et al. (2006a), we propose that, at this moment, wedge dynamics ceased, and Poiseuille flow started to prevail in an ~10-km-thick channel that decoupled from its lid and base and flowed toward the foreland. Between 90 and 70 Ma (Figs. 10A and 10B), the frontal part of the channel (location A on Figs. 1B and 3) cooled below the titanite closure temperature (600–650 °C) at pressures of 400–600 MPa as it flowed above an underthrusting basement ramp. Flow was

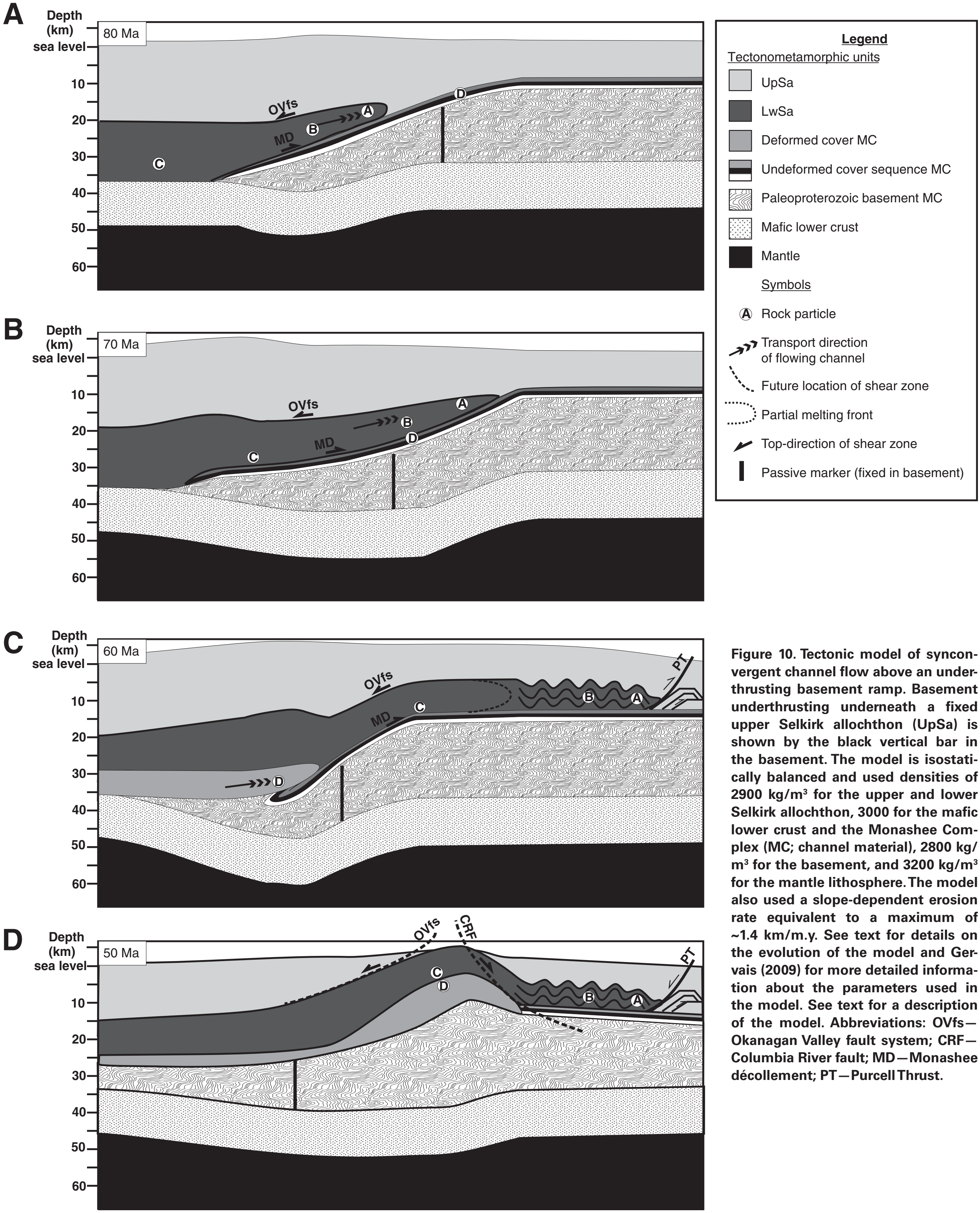

Figure 10. Tectonic model of synconvergent channel flow above an underthrusting basement ramp. Basement underthrusting underneath a fixed upper Selkirk allochthon (UpSa) is shown by the black vertical bar in the basement. The model is isostatically balanced and used densities of 2900 kg/m³ for the upper and lower Selkirk allochthon, 3000 for the mafic lower crust and the Monashee Complex (MC; channel material), 2800 kg/m³ for the basement, and 3200 kg/m³ for the mantle lithosphere. The model also used a slope-dependent erosion rate equivalent to a maximum of ~1.4 km/m.y. See text for details on the evolution of the model and Gervais (2009) for more detailed information about the parameters used in the model. See text for a description of the model. Abbreviations: OVfs—Okanagan Valley fault system; CRF—Columbia River fault; MD—Monashee décollement; PT—Purcell Thrust.

accommodated by internal ductile deformation within the channel and by top-to-the-E and top-to-the-W shearing along the Monashee décollement and the Okanagan Valley fault system, respectively. The southwest lateral trend of cooling ages (Figs. 3B and 9) suggests that basement underthrusting under a flowing channel continued for at least 30 m.y., between 90 and 60 Ma, while rocks of the Monashee Complex were progressively buried to a depth >35 km (1000 MPa; Fig. 3C). As mentioned already here and in Gervais et al. (2010), data from the Frenchman Cap dome indicate that basement underthrusting took place until 52–59 Ma. We propose a model similar to that of numerical model HT111 (Fig. 2B; Jamieson et al., 2006), in which the leading edge of the underthrusting indentor is expelled back above its stiffer part once it has been thermally softened. In the Monashee Complex, this would have occurred at ca. 58 Ma, when underthrusted cover sequence and basement rocks reached partial melting conditions (Figs. 3C and 10C). This model provides a mechanism to juxtapose rocks of the Monashee Complex and the lower Selkirk allochthon, which were then separated by more than 25 vertical km (compare Figs. 3C and 6). Postorogenic extension occurred at 50–47 Ma and was first accommodated in the brittle-ductile regime by the development of the Columbia River fault and the reactivation of the Okanagan Valley fault system (Fig. 10D), and then in the brittle regime by the formation of N-S–striking normal faults and the intrusion of lamprophyre dikes. Regional extension is well recorded by the cluster of mica cooling ages (Fig. 3B) and the timing of late shearing along the two main normal brittle-ductile shear zones, Columbia River fault and Okanagan Valley fault system (Table 2). It is noteworthy that this model is compatible with the palinspastic restoration of Johnson and Brown (1996), which implies significant exhumation of the lower Selkirk allochthon and Monashee Complex prior to 20%–25% extension.

In contrast with channel-flow models (Beaumont et al., 2001, 2004), erosion was most likely not a major driving force in the southeastern Canadian Cordillera. Low denudation rates in the Late Cretaceous are indicated by the study of Sears (2001), who coupled low-temperature thermochronology with palinspastic restoration, and are indicated by the large gap of ~20 m.y. between hornblende and mica cooling ages in the northern Monashee Mountains. We rather suggest that most of the exhumation was due to structural decoupling at the top of a channel flowing up an incline plane, and that part of the space was created by shortening in the foreland belt (Figs. 10B and 10C). This is supported by the synchronicity of the main shortening phase in the foreland belt and the exhumation of the channel between 75 and 59 Ma (Price and Sears, 2000; this study). With low denudation rates, we postulate that the main driving force was tectonic forcing by the underthrusting basement indentor, as reproduced in numerical models (Jamieson et al., 2006, 2010; Beaumont et al., 2010).

Consequently, a model of synconvergent channel flow and ductile intrusion above an underthrusting basement ramp reconciles all structural, metamorphic, and geochronological data available at the latitude of the Monashee Complex (Fig. 10). This region of the southeastern Canadian Cordillera thus constitutes a compelling natural analogue to the thermomechanical numerical models of channel flow (Beaumont et al., 2001, 2004, 2006; Jamieson et al., 2004, 2006, 2007, 2010).

CONCLUSIONS

1. We derived a test to distinguish among the main modes of exhumation in collisional orogens: orogenic wedge, channel flow, and gravitational collapse. The spatial distribution of finite strain patterns, cooling ages, and *P-T-t* paths as well as metamorphic field gradients and the timing of motion along reverse and normal shear zones can be used as a set of diagnostic criteria, whereas the shape of pressure-temperature (*P-T*) paths and absolute peak *P-T* conditions are not distinctive (Fig. 2).

2. Based on a new compilation of field-based data (Table 2), we propose a tectonometamorphic subdivision for studies focusing on high-grade rocks of the southeastern Canadian Cordillera. Hence, the crustal architecture consists of three main units stacked over each other (Figs. 1B and 3A) and includes, from upper to lower structural levels: the upper and lower Selkirk allochthon, and the Monashee Complex.

3. The commonly held view that exhumation of the high-grade core occurred by postconvergent gravitational collapse (Coney and Harms, 1984; Parrish et al., 1988; Vanderhaeghe and Teyssier, 1997; Teyssier and Whitney, 2002; Teyssier et al., 2005; Rey et al., 2009) is rejected because it fails our test. Notably, the prevalence of reverse shear strain rather than the predicted horizontal flattening (Fig. 3A), the exhumation of the lower Selkirk allochthon coeval with burial of the Monashee Complex in the Late Cretaceous to Paleocene (Fig. 9), the presence of 52–49 Ma contractional structures in the lower part of the Monashee Complex, and the absence of a penetrative foliation in the core of complex (Fig. 3A; Gervais et al., 2010) are strong arguments against this exhumation mode (Fig. 2C).

4. The absence of a steep flattening fabric (Fig. 3A), the sharp metamorphic field gradient between the lower Selkirk allochthon and the upper Selkirk allochthon across the Okanagan Valley fault system, and the coeval motion of major normal and reverse shear zones are characteristics difficult to reconcile with the orogenic wedge mode of exhumation (Fig. 2A).

5. In contrast, all the key requirements of the synconvergent model of channel flow are fulfilled (Fig. 2B). Notably: (1) the lower Selkirk allochthon is an 8–10-km-thick panel consisting of >30%–50% leucocratic material (leucosome + sheared leucogranite) bounded by reverse-sense and normal-sense shear zones at its base and roof, respectively, both of which were active together from at least the Paleocene (62–57 Ma) and probably since ca. 100–90 Ma (Table 7); (2) rocks of the upper Selkirk allochthon that surround the lower Selkirk allochthon had been exhumed to upper-crustal levels by the Late Cretaceous (Fig. 3B); (3) the lower Selkirk allochthon records a lateral gradient of cooling ages that become younger from the front to the rear of the proposed channel (Fig. 3B); and (4) footwall rocks of the proposed channel (i.e., the Monashee Complex) were being buried during synkinematic exhumation of the lower Selkirk allochthon (Fig. 9).

6. The database presented in Table 2 is internally consistent with a model of exhumation by channel flow above an underthrusting basement (Fig. 10).

APPENDIX

Analytical Methods for U-Pb Geochronology

Zircon and titanite grains were isolated using standard mineral separation techniques. Grains were mounted in epoxy and polished to reveal their centers. Cathodoluminescence (CL) imaging was conducted at Carleton University with an Electron Optics Services system interfaced to the Camebax microprobe, consisting of a high-sensitivity photo-multiplier (PM) tube connected to a Baush and Lomb CL amplifier. Images were collected at 15 kV accelerating potential and 15 nA beam current. Backscattered electron (BSE) images of the polished titanite were acquired with an electron microprobe (EMP) at the Massachusetts Institute of Technology with a JEOL 733 Superprobe, an accelerating voltage of 15 KeV, and beam current of 30 nA.

Isotopic data were acquired by laser ablation–multiple collector–inductively coupled plasma–mass spectrometry (LA-MC-ICP-MS) at the radiogenic isotope facility (RIF) of the University of Alberta, Edmonton. Instrumentation includes a Nu Plasma LA-MC-ICP-MS, coupled to a Nd:YAG UP213 laser ablation system. The LA-MC-ICP-MS instrument is equipped with a modified collector block containing 12 Faraday collectors and three ion counters (Simonetti et al., 2005). Raw data were normalized against the zircon standard FC-1 (ca. 1098 Ma) and titanite standard Khan (ca. 521 Ma; Simonetti et al., 2006). Additional analytical protocol and instrumentation are described in Simonetti et al. (2006). Errors are given at

2σ. Plots were made with Isoplot 3 (Ludwig, 2008). Using a 40 × 40 μm laser spot typically provided space for one or two analyses per grain. For a few analyses of small areas, labeled with asterisks in Tables 3 and 4, a 20 μm laser spot was used.

Because few studies have used LA-MC-ICP-MS to date titanite, it is important to evaluate the accuracy and precision obtained on the standard BLR-1, dated by Aleinikoff et al. (2007) at 1047.1 ± 0.4 Ma, which was routinely analyzed along with the unknowns. Three methods exist to correct for the large amount of common Pb typically present in titanite (Aleinikoff et al., 2004; Storey et al., 2006). The first regresses the uncorrected data on a Tera-Wasserburg semi–total Pb plot. If the data form an isochron, the intercept on the *y*-axis is assumed to yield the initial common Pb ratio, whereas the lower intercept on the concordia curve yields the age of the titanite. The second method calculates the weighted mean average of individual ^{206}Pb/^{238}U dates corrected with the Age7corr algorithm in Isoplot 3 (Ludwig, 2008), using the *y*-intercept on the Tera-Wasserburg plot and its uncertainty for the common Pb correction. If the analyses do not yield an isochron, the common Pb can be estimated from Stacey and Kramers (1975). The second and third methods have the disadvantage of assuming concordancy of the analyses, but they yield better precision. After discarding one of the 11 analyses of BLR-1 standard, which was clearly off the regression line on the Tera-Wasserburg plot, we found an age of 1041 ± 110 Ma (MSWD = 0.79; prob. = 0.62) using the first method and a weighted mean average of 1043 ± 35 Ma (MSWD = 0.09; prob. = 1.00) using the second method, both of which are in agreement with the true age.

ACKNOWLEDGMENTS

This work is part of a Ph.D. thesis conducted by FG under the supervision of RLB. The project was financed by a Natural Sciences and Engineering Research Council of Canada (NSERC) Discovery grant held by RLB. A. Simonetti of the Radiogenic Isotopic Facility of University of Alberta is thanked for his assistance during the acquisition of U-Pb LA-MC-ICP-MS data. We are grateful to S. Bowring from the Massachusetts Institute of Technology for providing access to his mineral separation laboratory, and particularly to J. Crowley, whose help in the field and in the geochronological labs was invaluable. D. Vachon is thanked for excellent field assistance. Numerous drafts of this manuscript were carefully edited and considerably improved by S. Carr and J. Percival. Critical constructive reviews by one anonymous reviewer and editorial handling by R. Russo significantly improved this manuscript. Two other anonymous reviewers are also thanked.

REFERENCES CITED

Aleinikoff, J.N., Horton, J.W., Drake, A.A., Wintsch, R.P., Fanning, C.M., Yi, K., Tollo, R.P., Corriveau, L., McLelland, J., and Bartholomew, M.J., 2004, Deciphering multiple Mesoproterozoic and Paleozoic events recorded in zircon and titanite from the Baltimore Gneiss, Maryland: SEM imaging, SHRIMP U-Pb geochronology, and EMP analysis, *in* Tollo, R.P., McLelland, J., Corriveau, L., and Bartholomew, M.J., eds., Proterozoic Tectonic Evolution of the Grenville Orogen in North America: Geological Society of America Memoir 197, p. 411–434.

Aleinikoff, J.N., Wintsch, R.P., Tollo, R.P., Unruh, D.M., Fanning, C.M., and Schmitz, M.D., 2007, Ages and origins of rocks of the Killingworth Dome, south-central Connecticut: Implications for the tectonic evolution of southern New England: American Journal of Science, v. 307, p. 63–118, doi:10.2475/01.2007.04.

Armstrong, R.L., Parrish, R.R., van der Heyden, P., Scott, K., Runkle, D., Brown, R.L., and Ross, G.M., 1991, Early Proterozoic basement exposures in the southern Canadian Cordillera: Core gneiss of Frenchman Cap, Unit I of the Grand Forks Gneiss, and the Vaseaux Formation: Canadian Journal of Earth Sciences, v. 28, p. 1169–1201, doi:10.1139/e91-107.

Bardoux, M., 1993, The Okanagan Valley Normal Fault from Penticton to Enderby, South-Central British Columbia [Ph.D. thesis]: Ottawa, Carleton University, 292 p.

Bardoux, M., and Mareschal, J., 1994, Extension in south-central British Columbia: Mechanical and thermal controls: Tectonophysics, v. 238, p. 451–470, doi:10.1016/0040-1951(94)90068-X.

Batt, G.E., and Braun, J., 1999, The tectonic evolution of the Southern Alps, New Zealand: Insights from fully thermally coupled dynamical modelling: Geophysical Journal International, v. 136, p. 403–420, doi:10.1046/j.1365-246X.1999.00730.x.

Beaumont, C.J., Jamieson, R.A., Nguyen, M.H., and Lee, B., 2001, Himalayan tectonics explained by extrusion of a low-viscosity crustal channel coupled to focused surface denudation: Nature, v. 414, p. 738–742, doi:10.1038/414738a.

Beaumont, C.J., Jamieson, R.A., Nguyen, M.H., and Medvedev, S., 2004, Crustal channel flows: 1. Numerical models with applications to the tectonics of the Himalayan-Tibetan orogen: Journal of Geophysical Research, v. 109, B06406, doi:10.1029/2003JB002809.

Beaumont, C.J., Nguyen, M.H., Jamieson, R.A., and Ellis, S., 2006, Crustal flow modes in large hot orogens, *in* Law, R.D., Searle, M.P., and Godin, L., eds., Channel flow, ductile extrusion and exhumation in continental collision zones: Geological Society of London Special Publication 268, p. 91–145, doi:10.1144/GSL.SP.2006.268.01.05.

Beaumont, C.J., Jamieson, R.A., and Nguyen, M.H., 2010, Models of large, hot orogens containing a collage of reworked and accreted terranes: Canadian Journal of Earth Sciences, v. 47, p. 485–515, doi:10.1139/E10-002.

Boggs, K.J.E., 2004, The Nature and Timing of Movement along the Purcell Thrust, Rocky Mountain Trench, British Columbia [Ph.D. thesis]: Calgary, University of Calgary, 486 p.

Bonnet, C., Malavieille, J., and Mosar, J., 2008, Surface processes versus kinematics of thrust belts: Impact on rates of erosion, sedimentation, and exhumation—Insights from analogue models: Bulletin de la Société Géologique de France, v. 179, p. 297–314, doi:10.2113/gssgfbull.179.3.297.

Brown, R.L., 2004, Thrust-belt accretion and hinterland underplating of orogenic wedges: An example from the Canadian Cordillera, *in* McClay, K.R., eds, Thrust Tectonics and Hydrocarbon Systems: American Association of Petroleum Geologists (AAPG) Memoir 82, p. 51–64.

Brown, R.L., and Gibson, H.D., 2006, An argument for channel flow in the southern Canadian Cordillera and comparison with Himalayan tectonics, *in* Law, R.D., Searle, M.P., and Godin, L., eds., Channel Flow, Ductile Extrusion and Exhumation in Continental Collision Zones: Geological Society of London Special Publication 268, p. 543–559.

Brown, R.L., and Journeay, J.M., 1987, Tectonic denudation of the Shuswap metamorphic terrane of southeastern British Columbia: Geology, v. 15, p. 142–146, doi:10.1130/0091-7613(1987)15<142:TDOTSM>2.0.CO;2.

Brown, R.L., and Willett, S.D., 1993, Comparison of the Selkirk fan structure with mechanical models: Implications for interpretation of the southern Canadian Cordillera: Geology, v. 21, p. 1015–1018, doi:10.1130/0091-7613(1993)021<1015:COTSFS>2.3.CO;2.

Brown, R.L., Carr, S.D., Johnson, B.J., Coleman, V.J., Cook, F.A., and Varsek, J.L., 1992, The Monashee décollement of the southern Canadian Cordillera: A crustal-scale shear zone linking the Rocky Mountain foreland belt to lower crust beneath accreted terranes, *in* McClay, K.R., ed., Thrust Tectonics: London, UK, Chapman & Hall, p. 357–364.

Brun, J.P., Sokoutis, D., and van den Driessche, J., 1994, Analogue modeling of detachment fault systems and core complexes: Geology, v. 22, p. 319–322, doi:10.1130/0091-7613(1994)022<0319:AMODFS>2.3.CO;2.

Burianyk, M.J.A., Kanasewich, E.R., 1995, Crustal velocity structure of the Omineca and Intermontane belts, southeastern Canadian Cordillera: Journal of Geophysical Research, v. 100, p. 15,303–15,316.

Carr, S.D., 1991, Three crustal zones in the Thor-Odin-Pinnacles area, southern Omineca belt, British Columbia: Canadian Journal of Earth Sciences, v. 28, p. 2003–2023.

Carr, S.D., 1992, Tectonic setting and U-Pb geochronology of the early Tertiary Ladybird leucogranite suite, Thor-Odin-Pinnacles area, southern Omineca belt, British Columbia: Tectonics, v. 11, p. 258–278, doi:10.1029/91TC01644.

Carr, S.D., 1995, The southern Omineca belt, British Columbia: New perspectives from the Lithoprobe Geoscience Program: Canadian Journal of Earth Sciences, v. 32, p. 1720–1739, doi:10.1139/e95-135.

Carr, S.D., and Simony, P.S., 2006, Ductile thrusting versus channel flow in the southeastern Canadian Cordillera; evolution of a coherent crystalline thrust sheet, *in* Law, R.D., Searle, M.P., and Godin, L., eds., Channel Flow, Ductile Extrusion and Exhumation in Continental Collision Zones: Geological Society of London Special Publication 268, p. 561–587.

Cherniak, D.J., 1993, Pb diffusion in titanite and preliminary results on the effects of radiation damage on Pb transport: Chemical Geology, v. 110, p. 177–194, doi:10.1016/0009-2541(93)90253-F.

Colpron, M., 1997, Stratigraphy, Structure and Thermotectonic Evolution of the Western Flank of the Selkirk Fan Structure, Northern Selkirk Mountains, British Columbia [Ph.D. thesis]: Kingston, Queen's University, 162 p.

Colpron, M., Price, R.A., Archibald, D.A., and Carmichael, D.M., 1996, Middle Jurassic exhumation along the western flank of the Selkirk fan structure: Thermobarometric and thermochronometric constraints from the Illecillewaet synclinorium, southeastern British Columbia: Geological Society of America Bulletin, v. 108, p. 1372–1392, doi:10.1130/0016-7606(1996)108<1372:MJEATW>2.3.CO;2.

Colpron, M., Price, R.A., and Archibald, D.A., 1999, ^{40}Ar/^{39}Ar thermochronometric constraints on the tectonic evolution of the Clachnacudainn Complex, southeastern British Columbia: Canadian Journal of Earth Sciences, v. 36, p. 1989–2006, doi:10.1139/cjes-36-12-1989.

Coney, P.J., and Harms, T.A., 1984, Cordilleran metamorphic core complexes: Cenozoic extensional relics of Mesozoic compression: Geology, v. 12, p. 550–554, doi:10.1130/0091-7613(1984)12<550:CMCCCE>2.0.CO;2.

Corfu, F., Hanchar, J.M., Hoskin, P.W.O., and Kinny, P.D., 2003, Atlas of zircon textures: Zircon: Reviews in Mineralogy and Geochemistry, v. 53, p. 469–500, doi:10.2113/0530469.

Crowley, J.L., 1999, U-Pb geochronological constraints on Paleozoic tectonism in the Monashee Complex, Canadian Cordillera: Elucidating an overprinted geologic history: Geological Society of America Bulletin, v. 111, p. 560–577, doi:10.1130/0016-7606(1999)111<0560:UPGCOP>2.3.CO;2.

Crowley, J.L., and Parrish, R.R., 1999, U-Pb isotopic constraints on diachronous metamorphism in the northern Monashee Complex, southern Canadian Cordillera: Journal of Metamorphic Geology, v. 17, p. 483–502, doi:10.1046/j.1525-1314.1999.00210.x.

Crowley, J.L., Ghent, E.D., and Brown, R.L., 1996, Metamorphism in the Clachnacudainn terrane and implications for tectonic setting in the southern Omineca belt, Canadian Cordillera: Canadian Journal of Earth Sciences, v. 33, p. 1570–1582.

Crowley, J.L., Brown, R.L., and Parrish, R.R., 2001, Diachronous deformation and a strain gradient beneath the Selkirk allochthon, northern Monashee Complex, southeastern

Canadian Cordillera: Journal of Structural Geology, v. 23, p. 1103–1121, doi:10.1016/S0191-8141(00)00179-6.

Crowley, J.L., Ghent, E.D., Carr, S.D., Simony, P.S., and Hamilton, M.A., 2003, Multiple thermotectonic events in a continuous metamorphic sequence, Mica Creek area, southeastern Canadian Cordillera: The American Mineralogist, v. 88, p. 930.

Crowley, J.L., Brown, R.L., Gervais, F., and Gibson, H.D., 2008, Assessing inheritance of zircon and monazite in granitic rocks: An example from the Monashee Complex, Canadian Cordillera: Journal of Petrology, v. 49, p. 1915–1929, doi:10.1093/petrology/egn047.

Currie, L.D., 1988, Geology of the Allan Creek Area, Cariboo Mountains, British Columbia [M.Sc. thesis]: Calgary, University of Calgary, 152 p.

Dahlen, F.A., 1990, Critical taper model of fold-and-thrust belts and accretionary wedges: Annual Review of Earth and Planetary Sciences, v. 18, p. 55–99, doi:10.1146/annurev.ea.18.050190.000415.

Digel, S.G., Ghent, E.D., Carr, S.D., and Simony, P.S., 1998, Early Cretaceous kyanite-sillimanite metamorphism and Paleocene sillimanite overprint near Mount Cheadle, southeastern British Columbia: Geometry, geochronology, and metamorphic implications: Canadian Journal of Earth Sciences, v. 35, p. 1070–1087, doi:10.1139/cjes-35-9-1070.

England, P.C., and Molnar, P., 1990, Surface uplift, uplift of rocks, and exhumation of rocks: Geology, v. 18, p. 1173–1177, doi:10.1130/0091-7613(1990)018<1173:SUUORA>2.3.CO;2.

Evenchick, C.A., McMechan, M.E., McNicoll, V.J., and Carr, S.D., 2007, A synthesis of the Jurassic–Cretaceous tectonic evolution of the central and southeastern Canadian Cordillera: Exploring links across the orogen, *in* Sears, J.W., Harms, T.A., and Evenchick, C.A., eds., Whence the Mountains? Inquiries into the Evolution of Orogenic Systems: A Volume in Honor of Raymond A. Price: Geological Society of America Special Paper 433, p. 117–145.

Foster, G., Parrish, R.R., Horstwood, M.S.A., Chenery, S., Pyle, J., and Gibson, H.D., 2004, The generation of prograde *P-T-t* points and paths; a textural, compositional, and chronological study of metamorphic monazite: Earth and Planetary Science Letters, v. 228, p. 125–142, doi:10.1016/j.epsl.2004.09.024.

Gervais, F., 2009, Pressure-Temperature-Time-Deformation Paths of Former Mid-Crustal Rocks, Northern Monashee Complex of the Southeastern Canadian Cordillera: A Model of Synconvergent Exhumation by Sequential Ductile Extrusion [Ph.D. thesis]: Ottawa, Carleton University, 325 p.

Gervais, F., and Brown, R.L., 2007, Sequential extrusive flow above a basement ramp documented from detailed *P-T-t-d* paths, Monashee Complex, SE Canadian Cordillera: Geological Society of America Abstracts with Programs, v. 39, no. 1, p. 78.

Gervais, F., Brown, R.L., and Crowley, J.L., 2010, Tectonic implications for a Cordilleran orogenic base in the Frenchman Cap dome, southeastern Canadian Cordillera: Journal of Structural Geology, v. 32, no. 7, p. 941–959, doi:10.1016/j.jsg.2010.05.006.

Ghent, E., and Villeneuve, M., 2006, ^{40}Ar/ ^{39}Ar dates on hornblende, muscovite, and biotite from the Mica Creek area, British Columbia; regional metamorphic and tectonic implications: Canadian Journal of Earth Sciences, v. 43, p. 83–100, doi:10.1139/e05-095.

Gibson, H.D., Brown, R.L., and Parrish, R.R., 1999, Deformation-induced inverted metamorphic field gradients: An example from the southeastern Canadian Cordillera: Journal of Structural Geology, v. 21, p. 751–767, doi:10.1016/S0191-8141(99)00051-6.

Gibson, H.D., Carr, S.D., Brown, R.L., and Hamilton, M.A., 2004, Correlations between chemical and age domains in monazite, and metamorphic reactions involving major pelitic phases: An integration of ID-TIMS and SHRIMP geochronology with Y-Th-U X-ray mapping: Chemical Geology, v. 211, p. 237–260, doi:10.1016/j.chemgeo.2004.06.028.

Gibson, H.D., Brown, R.L., and Carr, S.D., 2005, U-Th-Pb geochronological constraints on the structural evolution of the Selkirk fan, northern Selkirk Mountains, southern Canadian Cordillera: Journal of Structural Geology, v. 27, p. 1899–1924, doi:10.1016/j.jsg.2005.05.014.

Gibson, H.D., Brown, R.L., and Carr, S.D., 2008, Tectonic evolution of the Selkirk fan, southeastern Canadian Cordillera: A composite Middle Jurassic–Cretaceous orogenic structure: Tectonics, v. 27, TC6007, doi:10.1029/2007TC002160.

Gilley, L., 1999, The Nature and Timing of Partial Melting in the Shuswap Metamorphic Core Complex: A SHRIMP-RG Geochronological Investigation [Honor's thesis]: Stanford, California, Stanford University, 57 p.

Glombick, P.M., 2005, Mesozoic to Early Tertiary Tectonic Evolution of the Shuswap Metamorphic Complex in the Vernon Area, Southeastern Canadian Cordillera [Ph.D. thesis]: Edmonton, University of Alberta, 417 p.

Glombick, P., Thompson, R.I., Erdmer, P., and Daughtry, K.L., 2006a, A reappraisal of the tectonic significance of early Tertiary low-angle shear zones exposed in the Vernon map area (82 L), Shuswap metamorphic complex, southeastern Canadian Cordillera: Canadian Journal of Earth Sciences, v. 43, p. 245–268, doi:10.1139/E05-101.

Glombick, P., Thompson, R.I., Erdmer, P., Heaman, L., Friedman, R.M., Villeneuve, M., and Daughtry, K.L., 2006b, U-Pb constraints on the thermotectonic evolution of the Vernon antiform and the age of the Aberdeen gneiss complex, southeastern Canadian Cordillera: Canadian Journal of Earth Sciences, v. 43, p. 213–244, doi:10.1139/E05-096.

Goscombe, B.D., and Passchier, C.W., 2003, Asymmetric boudins as shear sense indicators: An assessment from field data: Journal of Structural Geology, v. 25, p. 575–589, doi:10.1016/S0191-8141(02)00045-7.

Grujic, D., 2006, Channel flow and continental collision tectonics: An overview, *in* Law, R.D., Searle, M.P., and Godin, L., eds., Channel flow, Ductile Extrusion and Exhumation in Continental Collision Zones: Geological Society of London Special Publication 268, p. 25–37.

Hanmer, S., and Passchier, C., 1991, Shear-Sense Indicators: A Review: Geological Survey of Canada Current Research 90-17, 72 p.

Hinchey, A.M., Carr, S.D., McNeill, P.D., and Rayner, N., 2006, Paleocene-Eocene high-grade metamorphism, anatexis, and deformation in the Thor-Odin dome, Monashee Complex, southeastern British Columbia: Canadian Journal of Earth Sciences, v. 43, p. 1341–1365, doi:10.1139/E06-028.

Hinchey, A.M., Carr, S.D., and Rayner, N., 2007, Bulk compositional controls on the preservation of age domains within metamorphic monazite: A case study from quartzite and garnet-cordierite-gedrite gneiss of Thor-Odin dome, Monashee Complex, Canadian Cordillera: Chemical Geology, v. 240, p. 85–102, doi:10.1016/j.chemgeo.2007.02.001.

Holdaway, M.J., 2001, Recalibration of the GASP geobarometer in light of recent garnet and plagioclase activity models and versions of the garnet-biotite geothermometer: The American Mineralogist, v. 86, p. 1117–1129.

Holland, T., and Blundy, J., 1994, Non-ideal interactions in calcite amphiboles and their bearing on amphibole-plagioclase thermometry: Contributions to Mineralogy and Petrology, v. 116, p. 433–447, doi:10.1007/BF00310910.

Jamieson, R.A., Beaumont, C.J., Fullsack, P., and Lee, B., 1998, Barrovian regional metamorphism: Where's the heat?, *in* Treloar, P.J., and O'Brien, P.J., eds., What Drives Metamorphism and Metamorphic Reactions?: Geological Society of London Special Publication 138, p. 23–51.

Jamieson, R.A., Beaumont, C.J., Nguyen, M.H., and Lee, B., 2002, Interaction of metamorphism, deformation and exhumation in large convergent orogens: Journal of Metamorphic Geology, v. 20, p. 9–24, doi:10.1046/j.0263-4929.2001.00357.x.

Jamieson, R.A., Beaumont, C.J., Medvedev, S., and Nguyen, M.H., 2004, Crustal channel flows: 2. Numerical models with implications for metamorphism in the Himalayan-Tibetan orogen: Journal of Geophysical Research, v. 109, B06407, doi:10.1029/2003JB002811.

Jamieson, R.A., Beaumont, C.J., Nguyen, M.H., and Grujic, D., 2006, Provenance of the Greater Himalayan Sequence and associated rocks; predictions of channel flow models, *in* Law, R.D., Searle, M.P., and Godin, L., eds., Channel Flow, Ductile Extrusion and Exhumation in Continental Collision Zones: Geological Society of London Special Publication 268, p. 165–182.

Jamieson, R.A., Beaumont, C.J., Nguyen, M.H., and Culshaw, N.G., 2007, Synconvergent ductile flow in variable-strength continental crust: Numerical models with application to the western Grenville orogen: Tectonics, v. 26, TC5005, doi:10.1029/2006TC002036.

Jamieson, R.A., Beaumont, C.J., Warren, C.J., and Nguyen, M.H., 2010, The Grenville orogen explained? Applications and limitations of integrating numerical models with geological and geophysical data: Canadian Journal of Earth Sciences, v. 47, p. 517–539, doi:10.1139/E09-070.

Johnson, B.J., 1994, Structure and Tectonic Setting of the Okanagan Valley Fault System in the Shuswap Lake Area, Southern British Columbia [Ph.D. thesis]: Ottawa, Carleton University, 266 p.

Johnson, B.J., 2006, Extensional shear zones, granitic melts, and linkage of overstepping normal faults bounding the Shuswap metamorphic core complex, British Columbia: Geological Society of America Bulletin, v. 118, p. 366–382, doi:10.1130/B25800.1.

Johnson, B.J., and Brown, R.L., 1996, Crustal structure and early Tertiary extensional tectonics of the Omineca belt at 51°N latitude, southern Canadian Cordillera: Canadian Journal of Earth Sciences, v. 33, p. 1596–1611, doi:10.1139/e96-121.

Johnston, D.H., Williams, P.F., Brown, R.L., Crowley, J.L., and Carr, S.D., 2000, Northeastward extrusion and extensional exhumation of crystalline rocks of the Monashee Complex, southeastern Canadian Cordillera: Journal of Structural Geology, v. 22, p. 603–625, doi:10.1016/S0191-8141(99)00185-6.

Journeay, J.M., 1986, Stratigraphy, Internal Strain and Thermo-Tectonic Evolution of Northern Frenchman Cap Dome: An Exhumed Duplex Structure, Omineca Hinterland, S.E. Canadian Cordillera [Ph.D. thesis]: Ottawa, Queen's University, 421 p.

Kohn, M.J., and Spear, F., 2000, Retrograde net transfer reaction insurance for pressure-temperature estimates: Geology, v. 28, p. 1127–1130, doi:10.1130/0091-7613(2000)28<1127:RNTRIF>2.0.CO;2.

Kretz, R., 1983, Symbols for rock-forming minerals: The American Mineralogist, v. 68, p. 277–279.

Kruse, S., 2007, Structural Evolution of the Northern Thor-Odin Culmination, Southern Canadian Cordillera [Ph.D. thesis]: Fredericton, University of New Brunswick, 373 p.

Kruse, S., and Williams, P.F., 2007, The Monashee reflection: Re-examination of a Lithoprobe crustal-scale seismic reflection in the southern Canadian Cordillera: Geosphere, v. 3, p. 26–41, doi:10.1130/GES00049.1.

Kuiper, Y.D., 2003, Isotopic Constraints on Timing of Deformation and Metamorphism in the Thor-Odin Dome, Monashee Complex, Southeastern British Columbia [Ph.D. thesis]: Fredericton, University of New Brunswick, 290 p.

Kuiper, Y.D., Kruse, S., and Williams, P.F., 2006, Possibility of channel flow in the southern Canadian Cordillera; a new approach to explain existing data, *in* Law, R.D., Searle, M.P., and Godin, L., eds., Channel Flow, Ductile Extrusion and Exhumation in Continental Collision Zones: Geological Society of London Special Publication 268, p. 589–611.

Lemieux, Y., 2006, Structure, Geochronology and Thermobarometry of the Eastern Flank of the Shuswap Metamorphic Complex in the Upper Arrow Lake Area, Southeastern British Columbia [Ph.D. thesis]: Edmonton, University of Alberta, 172 p.

Liu, M., 2001, Cenozoic extension and magmatism in the North American Cordillera: The role of gravitational collapse: Tectonophysics, v. 342, p. 407–433, doi:10.1016/S0040-1951(01)00173-1.

Lorencak, M., Seward, D., Vanderhaeghe, O., Teyssier, C., and Burg, J.P., 2001, Low-temperature cooling history of the Shuswap metamorphic core complex, British Columbia; constraints from apatite and zircon fission-track ages: Canadian Journal of Earth Sciences, v. 38, p. 1615–1625, doi:10.1139/cjes-38-11-1615.

Ludwig, K.R., 2008, User's Manual for Isoplot 3.6. A Geochronological Toolkit for Microsoft Excel: Berkeley Geochronological Center Special Publication 4, 78 p.

Malavieille, J., 2010, Impact of erosion, sedimentation, and structural heritage on the structure and kinematics of orogenic wedges: Analog models and case studies: GSA Today, v. 20, no. 1, p. 4–10, doi:10.1130/GSATG48A.1.

Marchildon, M.-F., 1999, Petrologic Studies of Process Interactions in Metamorphic Systems: Deformation and Metamorphism in the Selkirk Allochthon Orogenic Wedge and

Feedback Mechanisms during Reactive Fluid Flow [Ph.D. thesis]: Vancouver, University of British Columbia, 169 p.
McCarthy, T.C., and Patiño Douce, A.E., 1998, Empirical calibration of the silica-Ca-Tschermak's-anorthite (SCAn) geobarometer: Journal of Metamorphic Geology, v. 16, p. 675–686, doi:10.1111/j.1525-1314.1998.00164.x.
McNicoll, V.J., and Brown, R.L., 1995, The Monashee décollement at Cariboo Alp, southern flank of the Monashee Complex, southern British Columbia, Canada: Journal of Structural Geology, v. 17, p. 17–30, doi:10.1016/0191-8141(94)E0028-W.
Monger, J.W.H., Price, R.A., and Tempelman-Kluit, D.J., 1982, Tectonic accretion and the origin of the two major metamorphic and plutonic welts in the Canadian Cordillera: Geology, v. 10, p. 70–75, doi:10.1130/0091-7613(1982)10<70:TAATOO>2.0.CO;2.
Mulch, A., Teyssier, C., Cosca, M.A., and Vennemann, T.W., 2006, Thermomechanical analysis of strain localization in a ductile detachment zone: Journal of Geophysical Research, v. 111, B12405, doi:10.1029/2005JB004032.
Murphy, D.C., 1987, Suprastructure/infrastructure transition, east-central Cariboo Mountains, British Columbia: Geometry, kinematics and tectonic implications: Journal of Structural Geology, v. 9, p. 13–29, doi:10.1016/0191-8141(87)90040-X.
Norlander, B.H., Whitney, D.L., Teyssier, C., and Vanderhaeghe, O., 2002, Partial melting and decompression of the Thor-Odin dome, Shuswap metamorphic core complex, Canadian Cordillera: Lithos, v. 61, p. 103–125, doi:10.1016/S0024-4937(02)00075-0.
Nyman, M.W., Pattison, D.R.M., and Ghent, E.D., 1995, Melt extraction during formation of K-feldspar + sillimanite migmatites, west of Revelstoke, British Columbia: Journal of Petrology, v. 36, p. 351–372.
Parrish, R.R., 1995, Thermal evolution of the southeastern Canadian Cordillera: The Southern Canadian Cordillera transect of Lithoprobe: Canadian Journal of Earth Sciences, v. 32, p. 1618–1642, doi:10.1139/e95-130.
Parrish, R.R., Carr, S.D., and Parkinson, D.L., 1988, Eocene extensional tectonics and geochronology of the southern Omineca belt, British Columbia and Washington: Tectonics, v. 7, p. 181–212, doi:10.1029/TC007i002p00181.
Platt, J.P., 1986, Dynamics of orogenic wedges and the uplift of high-pressure metamorphic rocks: Geological Society of America Bulletin, v. 97, p. 1037–1053, doi:10.1130/0016-7606(1986)97<1037:DOOWAT>2.0.CO;2.
Powell, R., and Holland, T., 1994, Optimal geothermometry and geobarometry: The American Mineralogist, v. 79, p. 120–133.
Price, R.A., and Monger, J.W.H., 2003, A Transect of the Southern Canadian Cordillera from Calgary to Vancouver, May 2003: Vancouver, Geological Association of Canada, Cordilleran Section, 167 p.
Price, R.A., and Sears, J.W., 2000, A preliminary palinspastic map of the Mesoproterozoic Belt-Purcell Supergroup, Canada and USA: Implications for the tectonic setting and structural evolution of the Purcell anticlinorium and the Sullivan Deposit, *in* Lydon, J.W., Höy, T., Slack, J.F., and Knapp, M., eds., The Geological Environment of the Sullivan Deposit, British Columbia: Geological Association of Canada, Mineral Deposits Division, Special Publication 1, p. 61–81.
Raeside, R.P., and Simony, P.S., 1983, Stratigraphy and deformational history of the Scrip Nappe, Monashee Mountains, British Columbia: Canadian Journal of Earth Sciences, v. 20, p. 639–650.
Read, P.B., 1980, Stratigraphy and structure: Thor-Odin to Frenchman Cap "Domes," Vernon east-half map area, southern British Columbia: Current Research, Part A: Geological Survey of Canada Paper 79-1A, p. 19–25.
Read, P.B., and Brown, R.L., 1981, Columbia River fault zone: Southeastern margin of the Shuswap and Monashee Complexes, southern British Columbia: Canadian Journal of Earth Sciences, v. 18, p. 1127–1145.
Reid, L.F., 2002, Stratigraphy, Structure, Petrology, Geochronology and Geochemistry of the Hobson Lake Area (Cariboo Mountains, British Columbia) in Relation to the Tectonic Evolution of the Southern Canadian Cordillera [Ph.D. thesis]: Calgary, University of Calgary, 221 p.
Rey, P.F., Vanderhaeghe, O., and Teyssier, C., 2001, Gravitational collapse of the continental crust: Definition, regimes and modes: Tectonophysics, v. 342, p. 435–449, doi:10.1016/S0040-1951(01)00174-3.
Rey, P.F., Teyssier, C., and Whitney, D.L., 2009, Extension rates, crustal melting, and core complex dynamics: Geology, v. 37, p. 391–394, doi:10.1130/G25460A.1.
Ring, U., Brandon, M.T., Willett, S.D., and Lister, G.S., 1999, Exhumation processes, *in* Ring, U., Brandon, M.T., Willett, S.D., and Lister, G.S., eds., Exhumation Processes: Normal Faulting, Ductile Flow and Erosion: Geological Society of London Special Publication 154, p. 1–27.
Scammell, R.J., 1986, Stratigraphy, Structure and Metamorphism of the North Flank of the Monashee Complex, Southeastern British-Columbia: A Record of Proterozoic Extension and Phanerozoic Crustal Thickening [M.Sc. thesis]: Ottawa, Carleton University, 205 p.
Scammell, R.J., 1993, Mid-Cretaceous to Tertiary Thermotectonic History of Former Mid-Crustal Rocks, Southern Omineca Belt, Canadian Cordillera [Ph.D. thesis]: Kingston, Queen's University, 576 p.
Sears J.W., 2001, Emplacement and denudation history of the Lewis-Eldorado-Hoadley thrust slab in the northern Montana Cordillera, USA: Implications for steady-state orogenic processes: American Journal of Science, v. 301, p. 359–373.
Sevigny, J.H., Parrish, R.R., Donelick, R.A., and Ghent, E.D., 1990, Northern Monashee Mountains, Omineca crystalline belt, British Columbia: Timing of metamorphism, anatexis, and tectonic denudation: Geology, v. 18, p. 103–106, doi:10.1130/0091-7613(1990)018<0103:NMMOCB>2.3.CO;2.
Simonetti, A., Heaman, L.M., Hartlaub, R.P., Creaser, R.A., Machattie, T.G., and Böhm, C., 2005, U-Pb zircon dating by laser ablation-MC-ICP-MS using a new multiple ion counting Faraday collector array: Journal of Analytical Atomic Spectrometry, v. 20, p. 677–686, doi:10.1039/b504465k.
Simonetti, A., Heaman, L.M., Chacko, T., and Banerjee, N.R., 2006, In situ petrographic thin section U-Pb dating of zircon, monazite, and titanite using laser ablation-MC-ICP-MS: International Journal of Mass Spectrometry, v. 253, p. 87–97, doi:10.1016/j.ijms.2006.03.003.
Simony, P.S., Ghent, E.D., Craw, D., and Mitchell, W., 1980, Structural and metamorphic evolution of the northeast flank of the Shuswap Complex, southern Canoe River area, British Columbia, *in* Crittenden, M.D., Coney, P.J., and Davis, G.H., eds., Cordilleran Metamorphic Core Complexes: Geological Society of America Memoir 153, p. 445–461.
Spark, R.N., 2001, Crustal Thickening and Tectonic Denudation within the Thor-Odin Culmination, Monashee Complex, Southern Canadian Cordillera [Ph.D. thesis]: Fredericton, University of New Brunswick, 302 p.
Spear, F.S., 1993, Metamorphic Phase Equilibria and Pressure-Temperature-Time Paths: Washington, D.C., Mineralogical Society of America, 799 p.
Spear, F.S., Kohn, M.J., and Cheney, J.T., 1999, *P-T* paths from anatectic pelites: Contributions to Mineralogy and Petrology, v. 134, p. 17–32, doi:10.1007/s004100050466.
Stacey, J.S., and Kramers, J.D., 1975, Approximation of terrestrial lead isotope evolution by a two-stage model: Earth and Planetary Science Letters, v. 26, p. 207–221, doi:10.1016/0012-821X(75)90088-6.
Storey, C.D., Jeffries, T.E., and Smith, M., 2006, Common lead–corrected laser ablation ICP-MS U/Pb systematics and geochronology of titanite: Chemical Geology, v. 227, p. 37–52, doi:10.1016/j.chemgeo.2005.09.003.
Tempelman-Kluit, D., and Parkinson, D., 1986, Extension across the Eocene Okanagan crustal shear in southern British Columbia: Geology, v. 14, p. 318–321, doi:10.1130/0091-7613(1986)14<318:EATEOC>2.0.CO;2.
Teyssier, C., and Whitney, D.L., 2002, Gneiss domes and orogeny: Geology, v. 30, p. 1139–1142, doi:10.1130/0091-7613(2002)030<1139:GDAO>2.0.CO;2.
Teyssier, C., Whitney, D.L., Norlander, B., Ferré, E.C., Vanderhaeghe, O., and Parkinson, D., 2005, Flow of partially molten crust and origin of detachments during collapse of the Cordilleran orogen, *in* Bruhn, D., and Burlini, L., eds., High-Strain Zones: Structure and Physical Properties: Geological Society of London Special Publication 245, p. 39–64.
Tinkham, D., and Ghent, E.D., 2005, Estimating *P-T* conditions of garnet growth with isochemical phase diagram sections and the problem of effective bulk composition: Canadian Mineralogist, v. 43, p. 35–50, doi:10.2113/gscanmin.43.1.35.
Tirel, C., Brun, J.P., and Sokoutis, D., 2006, Extension of thickened and hot lithospheres: Inferences from laboratory modeling: Tectonics, v. 25, p. TC1005, doi:10.1029/2005TC001804.
Tirel, C., Gautier, D.J.J., Van Hinsbergen, D.J.J., and Wortel, M.J.R., 2009, Sequential development of interfering metamorphic core complexes: Numerical experiments and comparison with the Cyclades, Greece, *in* Van Hinsbergen, D.J.J., Edwards, M.A., and Govers, R., eds., Collision and Collapse at the Africa–Arabia–Eurasia Subduction Zone: Geological Society of London Special Publication 311, p. 257–292.
Unterschutz, J., 2002, Geological and Geochemical Links between Quesnel "Terrane" Strata and Ancestral North America, Southern Canadian Cordillera [M.Sc. thesis]: Edmonton, University of Alberta, 139 p.
Vanderhaeghe, O., and Teyssier, C., 1997, Formation of the Shuswap metamorphic core complex during late-orogenic collapse of the Canadian Cordillera: Geodinamica Acta, v. 10, p. 41–58.
Vanderhaeghe, O., Teyssier, C., and Wysoczanski, R., 1999, Structural and geochronological constraints on the role of partial melting during the formation of the Shuswap metamorphic core complex at the latitude of the Thor-Odin dome, British Columbia: Canadian Journal of Earth Sciences, v. 36, p. 917–943, doi:10.1139/cjes-36-6-917.
Vanderhaeghe, O., Medvedev, S., Fullsack, P., Beaumont, C.J., and Jamieson, R.A., 2003a, Evolution of orogenic wedges and continental plateaux: Insights from crustal thermal-mechanical models overlying subducting mantle lithosphere: Geophysical Journal International, v. 153, p. 27–51, doi:10.1046/j.1365-246X.2003.01861.x.
Vanderhaeghe, O., Teyssier, C., McDougall, I., and Dunlap, W.J., 2003b, Cooling and exhumation of the Shuswap metamorphic core complex constrained by ^{40}Ar/^{39}Ar thermochronology: Geological Society of America Bulletin, v. 115, p. 200–216, doi:10.1130/0016-7606(2003)115<0200:CAEOTS>2.0.CO;2.
Vernon, R.H., 2004, A Practical Guide to Rock Microstructure: Cambridge, UK, Cambridge University Press, 594 p.
Vielzeuf, D., and Schmidt, M.W., 2001, Melting relations in hydrous systems revisited: Application to metapelites, metagreywackes and metabasalts: Contributions to Mineralogy and Petrology, v. 141, p. 251–267, doi:10.1007/s004100100237.
Wheeler, J.O., and McFeely, P., 1991, Tectonic Assemblage Map of the Canadian Cordillera and Adjacent Parts of the United States of America: Geological Survey of Canada "A" Series Map 1712A, scale 1:2,000,000.
White, R.W., Powell, R., and Holland, T.J.B., 2007, Progress relating to calculation of partial melting equilibria for metapelites: Journal of Metamorphic Geology, v. 25, p. 511–527, doi:10.1111/j.1525-1314.2007.00711.x.
Whitney, D.L., Teyssier, C., and Vanderhaeghe, O., 2004, Gneiss domes and crustal flow, *in* Whitney, D.L., Teyssier, C., and Siddoway, C.S., eds., Gneiss Domes in Orogeny: Geological Society of America Special Paper 380, p. 15–33.
Willett, S.D., 1999a, Orogeny and orography: The effects of erosion on the structure of mountain belts: Journal of Geophysical Research, v. 104, p. 28,957–28,981.
Willett, S.D., 1999b, Rheological dependence of extension in wedge models of convergent orogens: Tectonophysics, v. 305, p. 419–435.
Willett, S.D., Beaumont, C.J., Fullsack, P., 1993, Mechanical model for the tectonics of doubly vergent compressional orogens: Geology, v. 21, p. 371–374, doi:10.1130/0091-7613(1993)021<0371:MMFTTO>2.3.CO;2.
Williams, P.F., and Jiang, D., 2005, An investigation of lower crustal deformation: Evidence for channel flow and its implications for tectonics and structural studies: Journal of Structural Geology, v. 27, p. 1486–1504, doi:10.1016/j.jsg.2005.04.002.

MANUSCRIPT RECEIVED 29 JANUARY 2010
REVISED MANUSCRIPT RECEIVED 21 SEPTEMBER 2010
MANUSCRIPT ACCEPTED 5 OCTOBER 2010

Printed in the USA